Article

Cell Reports

Bidirectional Control of Synaptic $GABA_AR$ Clustering by Glutamate and Calcium

Graphical Abstract

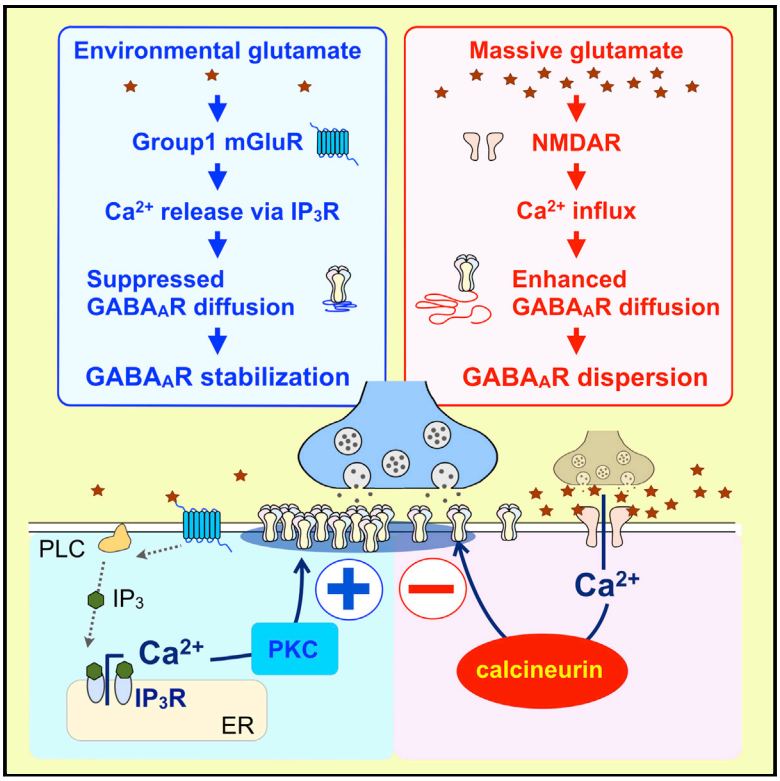

Highlights

- Bidirectional synaptic control system by glutamate and Ca^{2+} signaling
- Stabilization of GABA synapses by mGluR-dependent Ca^{2+} release from IP_3R via PKC
- Synaptic $GABA_AR$ clusters stabilized through regulation of $GABA_AR$ lateral diffusion
- Competition with an NMDAR-dependent Ca^{2+} pathway driving synaptic destabilization

Authors

Hiroko Bannai, Fumihiro Niwa, Mark W. Sherwood, ..., Sabine Lévi, Antoine Triller, Katsuhiko Mikoshiba

Correspondence

triller@biologie.ens.fr (A.T.), mikosiba@brain.riken.jp (K.M.)

In Brief

Bannai et al. characterize bidirectional regulation of synaptic $GABA_AR$ stability by glutamate and Ca^{2+}. Environmental glutamate continuously stabilizes synaptic $GABA_AR$ clusters through mGluR-dependent Ca^{2+} release through IP_3Rs and PKC activation. In contrast, massive glutamate induces $GABA_AR$ dispersion through the activation of NMDA receptor and calcineurin.

Bannai et al., 2015, Cell Reports *13*, 2768–2780
December 29, 2015
http://dx.doi.org/10.1016/j.celrep.2015.12.002

OPEN ACCESS
CellPress

Cell Reports
Article

Bidirectional Control of Synaptic $GABA_AR$ Clustering by Glutamate and Calcium

Hiroko Bannai,[1,2,3,4,6] Fumihiro Niwa,[1,6] Mark W. Sherwood,[1] Amulya Nidhi Shrivastava,[4] Misa Arizono,[1] Akitoshi Miyamoto,[1] Kotomi Sugiura,[1] Sabine Lévi,[4,5] Antoine Triller,[4,7,*] and Katsuhiko Mikoshiba[1,7,*]

[1]Laboratory for Developmental Neurobiology, RIKEN Brain Science Institute (BSI), 2-1 Hirosawa, Wako, Saitama 351-0198, Japan
[2]Division of Biological Science
[3]Nagoya Research Center for Brain & Neural Circuits
Graduate School of Science, Nagoya University, Furo-cho, Chikusa, Nagoya 464-8602, Japan
[4]École Normale Supérieure, Institut de Biologie de l'ENS (IBENS), INSERM, CNRS, Ecole Normale Supérieure, PSL Research University, 46 rue d'Ulm, 75005 Paris, France
[5]Institut du Fer à Moulin, INSERM, Unité Mixte de Recherche-S 839, Sorbonne Universités, Université Pierre et Marie Curie, 75005 Paris, France
[6]Co-first author
[7]Co-senior author
*Correspondence: triller@biologie.ens.fr (A.T.), mikosiba@brain.riken.jp (K.M.)
http://dx.doi.org/10.1016/j.celrep.2015.12.002

SUMMARY

GABAergic synaptic transmission regulates brain function by establishing the appropriate excitation-inhibition (E/I) balance in neural circuits. The structure and function of GABAergic synapses are sensitive to destabilization by impinging neurotransmitters. However, signaling mechanisms that promote the restorative homeostatic stabilization of GABAergic synapses remain unknown. Here, by quantum dot single-particle tracking, we characterize a signaling pathway that promotes the stability of $GABA_A$ receptor ($GABA_AR$) postsynaptic organization. Slow metabotropic glutamate receptor signaling activates IP_3 receptor-dependent calcium release and protein kinase C to promote $GABA_AR$ clustering and GABAergic transmission. This $GABA_AR$ stabilization pathway counteracts the rapid cluster dispersion caused by glutamate-driven NMDA receptor-dependent calcium influx and calcineurin dephosphorylation, including in conditions of pathological glutamate toxicity. These findings show that glutamate activates distinct receptors and spatiotemporal patterns of calcium signaling for opposing control of GABAergic synapses.

INTRODUCTION

A dynamic balance between excitation and inhibition is crucial for brain functions, such as the generation of rhythmic cortical network activities (Haider et al., 2006; Mann and Mody, 2010) and regulation of the critical period (Hensch, 2004). Accordingly, imbalances may result in neurological disorders like epilepsy and neuropsychiatric diseases like autism (Eichler and Meier, 2008; Yizhar et al., 2011). Extensive evidence indicates that inhibitory GABAergic synaptic transmission plays a key role in the regulation of excitation-inhibition (E/I) balance (Mann and Paulsen, 2007). Thus, understanding the molecular mechanisms regulating GABAergic synaptic transmission, which remain unclear compared to excitatory synapses, is crucial for understanding basic brain function in health and disease.

Fast GABAergic inhibition, i.e., $GABA_A$ receptor ($GABA_AR$)-mediated inhibitory synaptic transmission, critically depends on the degree of $GABA_AR$ clustering that determines the total number of synaptic $GABA_ARs$ (Kilman et al., 2002; Nusser et al., 1997). Clustering is regulated by the balance between endocytosis and exocytosis (Luscher et al., 2011) and rapid receptor exchange in and out of synapses by lateral diffusion on the cell surface (Triller and Choquet, 2008). In hippocampal neurons, GABAergic inhibition is plastically modulated by neuronal activities through the control of $GABA_AR$ diffusion and clustering (Gaiarsa et al., 2002; Luscher et al., 2011; Petrini and Barberis, 2014). Phasic and sustaining Ca^{2+} influx through *N*-Methyl D-aspartic acid (NMDA)-gated ionotropic glutamate receptors (NMDARs) induces long-term depression of GABAergic transmission (iLTD), which results from an increase in $GABA_AR$ lateral diffusion and the synaptic escape of $GABA_AR$ due to calcineurin-dependent dephosphorylation of the $GABA_AR$ γ2 subunit at the residue serine 327 (Bannai et al., 2009; Luscher et al., 2011; Muir et al., 2010; Niwa et al., 2012). A different context of transient NMDA stimulation evokes GABAergic long-term potentiation (iLTP) through synaptic translocation of Ca^{2+}-Calmodulin-dependent kinase II (CaMKII) that leads to phosphorylation of $GABA_AR$ β3 serine 383 and stabilization of synaptic $GABA_AR$ (Marsden et al., 2010; Petrini et al., 2014). Although detailed molecular mechanism for plastic changes of GABAergic synapses are well characterized, a homeostatic mechanism for the maintenance of GABAergic synapses during continuous exchange of receptors by lateral diffusion and the recovery of $GABA_AR$ clusters after dispersion (Niwa et al., 2012) remains unidentified.

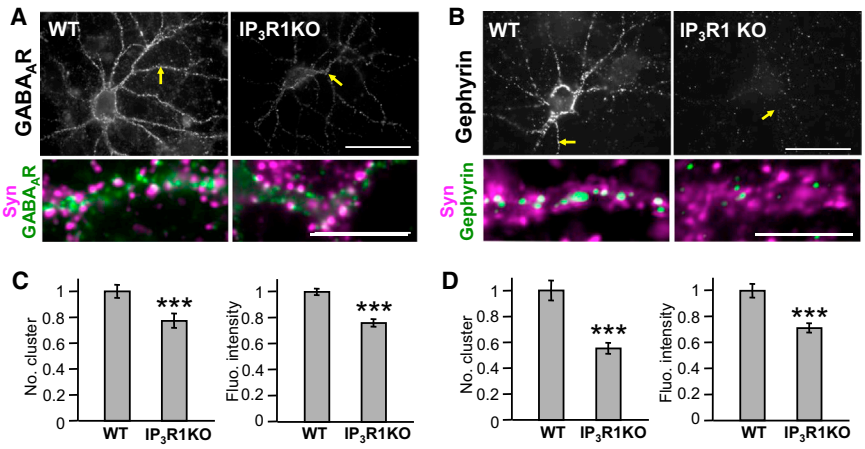

Figure 1. Gene KO of IP_3R1 Conducts to the Dispersal of $GABA_AR$ and Gephyrin Clusters

(A and B) Hippocampal neurons from 15–18 DIV wild-type (WT) or IP_3R1 knockout (IP_3R1KO) mice stained for $GABA_AR$ γ2 subunit (A) and gephyrin (B). Arrows in upper panels indicate the dendrites enlarged in lower panels. Color code in lower panels is as follows: green, $GABA_AR$ or gephyrin clusters; magenta, synapsin punctae; and white, $GABA_AR$ or gephyrin clusters facing synapsin-labeled boutons. Note the decrease in $GABA_AR$ and gephyrin immunoreactivities in IP_3R1KO neurons as compared to WT neurons. Scale bars, 50 and 10 μm in upper and lower panels, respectively.

(C and D) Number of synaptic clusters per dendrite length (left) and fluorescent intensities (right) of synaptic $GABA_AR$ (C) and gephyrin (D) clusters. Values represent mean ± SEM and were normalized to their respective control values (C, n = 36 cells for WT, n = 38 for IP_3R1KO; D, n = 37 for WT, n = 38 for IP_3R1KO; ***$p < 0.005$, Welch's *t*-test).

We sought to identify and characterize the signaling pathway that continuously stabilizes GABAergic synaptic structure. For this purpose, we focused on the contribution of IP_3-induced Ca^{2+} release (IICR) from intracellular Ca^{2+} stores in the endoplasmic reticulum (ER) (Berridge, 1998) to GABA synaptic structure. IICR is critical for brain development and function, such as the control of neurite outgrowth, morphogenesis of dendrites, and motor coordination in vivo (Hisatsune et al., 2006, 2013; Matsumoto et al., 1996; Mikoshiba, 2011; Sugawara et al., 2013; Takei et al., 1998). Here we report that metabotropic glutamate receptor (mGluR)-dependent IICR mediates the homeostatic stabilization of $GABA_AR$ structures, opposing destabilization by Ca^{2+} influx through NMDA-type ionotropic glutamate receptors.

RESULTS

mGluR-Dependent Activation of IP_3 Receptors Stabilizes $GABA_AR$ Clusters at Inhibitory Synapses

Type 1 IP_3 receptor (IP_3R1) is the dominant IP_3R subtype in neurons (Furuichi et al., 1993). To study the impact of IICR on the GABAergic synapse, we investigated the postsynaptic clustering of $GABA_AR$ and of its scaffolding molecule gephyrin in hippocampal neurons cultured from IP_3R1 knockout (IP_3R1 KO) mice (Matsumoto et al., 1996). $GABA_AR$ and gephyrin were labeled using an antibody against the $GABA_AR$ γ2 subunit (Niwa et al., 2012) and commercial gephyrin antibodies, respectively. $GABA_AR$ and gephyrin clusters were considered synaptic when adjacent to synapsin-immunoreactive boutons (Bannai et al., 2009). We found that $GABA_AR$ γ2 (Figure 1A) and gephyrin (Figure 1B) immunoreactivities were reduced in IP_3R1 KO neurons compared with wild-type (WT) neurons (Figures 1A and 1B). Quantification revealed that both the number of $GABA_AR$ clusters per dendritic length and the fluorescent intensity of $GABA_AR$ clusters were significantly reduced in IP_3R1 KO neurons (75.4% ± 5.5% and 75.6% ± 3.2% of WT, respectively; Figure 1C). The number of gephyrin clusters per dendrite length and the fluorescent intensity of gephyrin clusters in IP_3R1 KO neurons were 55.4% ± 4.2% and 71.3% ± 3.7% of WT neurons, respectively (Figure 1D). However, we found a 19.7% ± 3.5% reduction in the number of synapsin-immunoreactive terminals per dendrite length in IP_3R1KO neurons, suggesting that the persistent loss of IICR impaired synaptic connectivity.

We therefore examined the impact of IICR on $GABA_AR$ and gephyrin following acute blockade of IP_3R with 2-aminoethoxydiphenyl borate (2APB, 100 μM) (Maruyama et al., 1997). The fluorescence intensity of postsynaptic $GABA_AR$ clusters was not different in neurons exposed for 30 min to 2APB as compared to untreated cells (Figures 2A and 2B). It was only after 60–90 min of drug exposure that the fluorescence intensity, but not the number of synaptic $GABA_AR$ clusters per dendrite length, was significantly reduced (Figures 2A and 2B). Considering that neuronal excitation-dependent Ca^{2+} influx induces the dispersion of $GABA_AR$ clusters (Bannai et al., 2009; Muir et al., 2010), loss of IICR could affect the GABAergic synapses through the enhancement of neuronal excitation and Ca^{2+} influx. This possibility was excluded by the findings that 2APB reduced the fluorescence intensity of $GABA_AR$ clusters when action potentials (APs) were blocked with tetrodotoxin (TTX, 1 μM) (Figures S1A and S1B) or when extracellular Ca^{2+} was removed by Chelex (Figures S1C and S1D), indicating that IICR regulates $GABA_AR$ clustering in basal condition and in the absence of Ca^{2+} influx.

We then checked whether 2APB alters other key constituents of the inhibitory synapse, such as the main scaffolding molecule gephyrin. We found that 60 min of 2APB treatment decreased both the number and fluorescence intensity of gephyrin clusters (Figures 2C and 2D), indicating a global impact of 2APB on the molecular organization of the GABA synapse. The shrinkage of gephyrin clusters also was confirmed by time-lapse imaging of cultured hippocampal neurons from mRFP-gephyrin knockin mice (Calamai et al., 2009) treated with 2APB (Figure S2). We recently demonstrated that gephyrin was stabilized at synapses through its interaction with $GABA_AR$ (Niwa et al., 2012). Similarly, we show here that $GABA_AR$ antibody cross-linking prevented the dispersion of gephyrin clusters by 2APB (Figure S3), suggesting that the loss of gephyrin at synapses was secondary to the receptor dispersal.

IP_3Rs located at the surface of the ER are often activated via the production of phospholipase C (PLC) following the activation of group I mGluRs. We therefore examined the impact of this signaling pathway on $GABA_AR$ and gephyrin clustering following acute blockade of PLC and mGluR with U73122 (1 μM) and α-methyl-4-carboxyphenylglycine (MCPG, 250 μM), respectively. U73122 and MCPG impaired the clustering of both $GABA_AR$ and gephyrin after 60–90 min of drug exposure (Figure S4; Figure 2D). We thus checked whether mGluR activation stabilizes GABA synapses. We showed that acute IICR activation by group I mGluR agonist dihydroxyphenylglycine (DHPG, 5 μM) increased the intracellular Ca^{2+} level, as observed with Ca^{2+} imaging (Figure 2E). Furthermore, acute DHPG treatment (10–40 min) increased the fluorescence intensity of synaptic $GABA_AR$ clusters by 17%–26% (Figures 2F and 2G), indicating that Ca^{2+} release from ER stores indeed promotes $GABA_AR$ clustering. Altogether, these results indicate that mGluR-dependent IICR constitutively stabilizes the post-synaptic clustering of $GABA_ARs$ and gephyrin.

Impact of mGluR Signaling on $GABA_AR$-Mediated Synaptic Transmission

Since a loss of synaptic $GABA_AR$ is often correlated with reduced synaptic efficacy (Kilman et al., 2002; Nusser et al., 1997, 1998), we checked whether IICR inhibition impacts GABAergic synaptic transmission. We recorded inward $GABA_AR$-mediated miniature inhibitory postsynaptic currents (mIPSCs) in the presence of TTX and ionotropic glutamate receptor antagonists in cultured hippocampal neurons, with and without MCPG treatment (60- to 90-min incubation). Representative traces illustrate that MCPG reduced $GABA_AR$-mediated mIPSC amplitude (Figure 3A). The distribution of mIPSC amplitudes was significantly shifted toward lower values (Figure 3B). In contrast, the time to peak (Figure 3C) and decay time τ (Figure 3D) remained unchanged after MCPG treatment, indicating no impact of IICR on $GABA_AR$ channel kinetics. Furthermore, mIPSC amplitude was significantly reduced in post-natal day (P)14–P16 hippocampal slices derived from IP_3R1 KO mice as compared with WT animals (Figure 3E), with unchanged time to peak (Figure 3F) and slightly reduced decay time τ (Figure 3G). We thus concluded that the dispersal of $GABA_AR$ clusters following IICR blockade is responsible for the reduction in GABAergic synaptic efficacy.

Ca^{2+} Influx and Ca^{2+} Release Define Opposing Mechanisms to Control $GABA_AR$ Clustering

We previously showed that the NMDAR-mediated dispersal of synaptic $GABA_AR$ and gephyrin clustering was reversed 15 min after NMDA withdrawal (Bannai et al., 2009; Niwa et al., 2012; Figures 4A–4C). We show here that $GABA_AR$ clustering did not recover after NMDA removal when IICR was blocked with the IP_3R antagonist 2APB (Figures 4A and 4B) or the group I/II mGluR inhibitor MCPG (Figure 4C), suggesting IICR participates in the recovery phase. These results also suggest that Ca^{2+} influx and IICR operate through separate, non-overlapping mechanisms to regulate $GABA_AR$ clustering. We further examined whether recruitment of Ca^{2+} stores could prevent NMDAR and Ca^{2+} influx-mediated dispersion of $GABA_AR$ clusters. For this purpose, we applied DHPG together with NMDA to neurons pre-treated with NMDA. We found that activation of IICR did not reverse the NMDA-induced $GABA_AR$ loss of clusters when NMDA was applied first (Figures 4D–4F). In contrast, DHPG pre-treatment for 30 min completely prevented $GABA_AR$ dispersion (Figures 4G–4I). These results highlight that, when engaged, these two glutamatergic pathways cannot be antagonized by the activation of a secondary pathway.

Intracellular Calcium Scales $GABA_AR$ Clustering via Regulation of Lateral Diffusion

$GABA_AR$ undergoes extensive endocytosis through clathrin-dependent mechanisms (Kittler et al., 2004), and the density of $GABA_AR$ at synapses is largely dependent on the controlled removal of receptors from the plasma membrane (Kittler et al., 2008). However, we found 2APB was able to reduce $GABA_AR$ clustering, even when clathrin-dependent endocytosis was prevented by the membrane-permeant dynamin blocker dynasore (Newton et al., 2006; Figures S5A and S5B). We quantified the levels of total and surface $GABA_AR$ using surface biotinylation and western blot analysis. $GABA_AR$ was identified using a homemade antiserum directed against the β3 subunit, a subunit that assembles with the γ2 subunit at inhibitory synapses (Sieghart et al., 1999). The antiserum specificity was validated by western blot using protein extracts from hippocampal cultured neurons or HeLa cells transfected or not with the $GABA_AR$ β3 subunit together with the α2 and γ2 subunits (Figure S5C). Quantification of the amount of total and biotinylated surface $GABA_AR$ proteins (Jovanovic et al., 2004) in the presence or absence of 2APB (for 60 min) revealed no significant changes in the membrane and total pools of $GABA_AR$ (Figures S5D and S5E), suggesting that the loss of $GABA_AR$ at inhibitory synapses did not result from internalization and degradation of the receptor.

The regulation of receptor membrane dynamics contributes to the rapid control of their numbers at synapses (Choquet and Triller, 2013; Gerrow and Triller, 2010; Triller and Choquet, 2005, 2008). The activity-dependent reduction of $GABA_AR$ number at inhibitory synapses is due to a reduction in receptor diffusion constraints (Bannai et al., 2009; Bouthour et al., 2012; Muir et al., 2010). We thus examined the influence of IICR on the lateral diffusion of $GABA_AR$ using a quantum dot (QD)-based single-particle tracking (SPT) approach (Bannai et al., 2006; Lévi et al., 2011). Synaptic and extrasynaptic sub-trajectories were segregated according to their colocalization with FM4-64 punctae (Bannai et al., 2009). Neuronal exposure to 2APB apparently increased the surface exploration of individual trajectories within 30 min (Figure 5A). Indeed, diffusion coefficients of both extrasynaptic and synaptic QDs significantly increased (Figure 5B). However, the increase in diffusion was not associated with a significant change in the dwell time (Figure 5C) or size of the domain of confinement (Figure 5D) at inhibitory synapses, meaning 2APB did not lead to a noticeable loss of $GABA_AR$. It was after 60 min of 2APB application that the increase in diffusion coefficients (Figures 5E and 5F) was associated with a reduction in the dwell time (79.0% of control; Figure 5G) and an increase in the confinement size (120.5% of control; Figure 5H) at inhibitory synapses, indicative of synaptic escape.

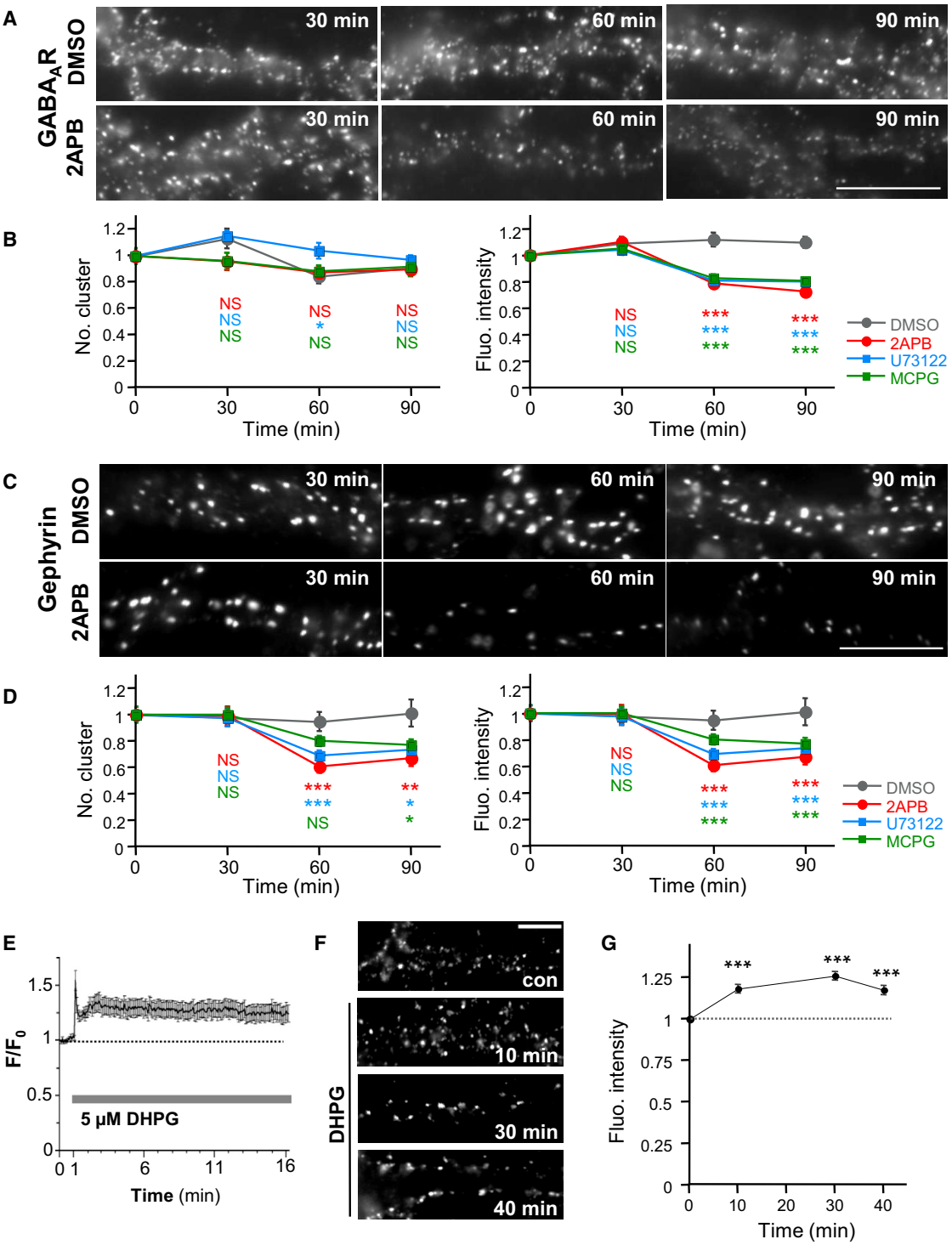

Figure 2. mGluR/IICR-Signaling Cascade Promotes Clustering of GABA$_A$R and Gephyrin

(A–D) Effect of pharmacological blockade of IICR on GABA$_A$R (A and B) and gephyrin (C and D) clustering in 21–27 DIV hippocampal neurons. (A and C) Representative examples show GABA$_A$R (A) or gephyrin (C) immunoreactivity after 100 µM 2APB or 0.1% DMSO treatment for 30, 60, and 90 min. (B and D) The number of cluster per dendrite length (left) and fluorescence intensities (right) of synaptic GABA$_A$R (B) or gephyrin (D) clusters in cells exposed to DMSO (gray), 2APB (red), U73122 (blue), or MCPG (green) are shown. Plots show mean values ± SEM in function of time. Data were normalized to their respective control values.

(legend continued on next page)

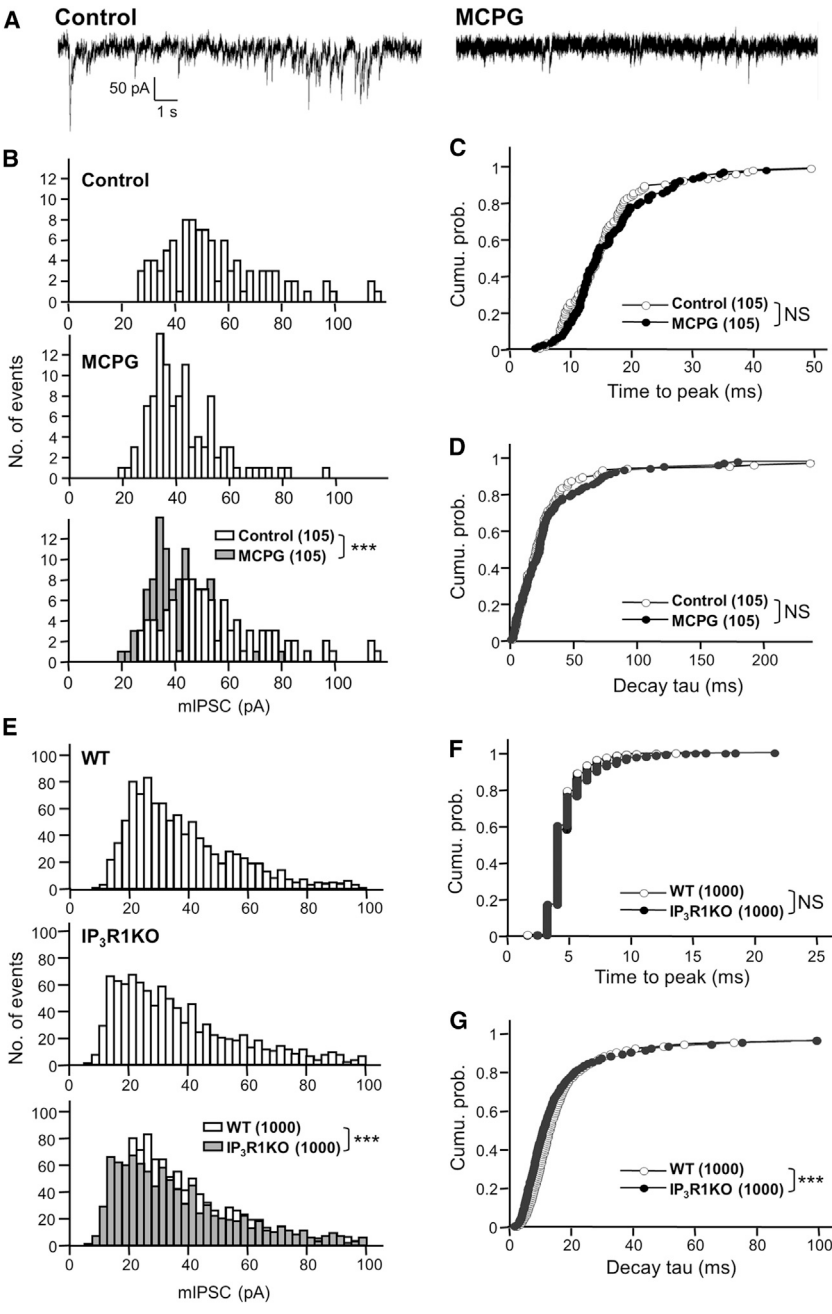

Figure 3. Lower Efficacy of GABA Synapses after Reduced IICR Activity

(A) Examples show GABAergic mIPSC traces recorded in cultured hippocampal neurons in the absence (left) or presence (right) of mGluR inhibitor MCPG.

(B) Distribution of mIPSC amplitudes in the absence (white, top and bottom) or presence (gray, middle and bottom) of MCPG. Note that the distribution of mIPSC amplitudes is shifted toward lower values in MCPG-treated neurons.

(C and D) Cumulative distributions of time to peak (C) and decay time constant (D) of mIPSCs in the absence (open) or presence of MCPG (close). The first 15 events were collected from seven neurons per condition.

(E) Distributions of mIPSC amplitudes recorded in pyramidal neurons from P14–P16 WT (white, top and bottom) or IP_3R1KO mice (gray, middle and bottom) hippocampal slices. The overlay emphasizes the reduction in mIPSC amplitudes in IP_3R1KO.

(F and G) Distributions of time to peak (F) and decay time constant (G) of mIPSCs of WT (white circle) and IP_3R1KO (black circle). The first 250 events were collected from four neurons per condition (***$p < 0.005$; ns, not significant; Mann-Whitney *U*-test).

A similar relief in $GABA_AR$ diffusion constraints was found in neurons derived from IP_3R1 KO animals as compared with WT neurons (Figures 5I–5L). Considering that 2APB (60–90 min) did not affect the membrane dynamics of mGluR5 (Figure S6), we concluded that the 2APB-dependent relief in diffusion constraints of the $GABA_AR$ was not due to a global effect on the properties of the membrane. Furthermore, neuronal exposure to MCPG also led to a faster synaptic escape of $GABA_AR$ (Figures 5M–5P), demonstrating that the mGluR-dependent IICR pathway regulates the surface mobility of $GABA_AR$. Altogether our results show that the IICR-signaling pathway constrains the diffusion of $GABA_AR$ during basal activity, maintaining a stable pool of $GABA_ARs$ at inhibitory synapses.

Counteracting Kinase-Phosphatase Systems Control $GABA_AR$ Diffusion

We found that the calcineurin inhibitor cyclosporin A or FK506 (CysA, 1 μM; FK506, 1 μM; Figure 5Q) completely prevented the effect of IICR blockade on $GABA_AR$ diffusion dynamics, i.e., the increase in diffusion coefficients at synaptic sites (Figure 5R), synaptic escape (Figure 5S), and synaptic confinement size (Figure 5T). These results suggest that basal calcineurin activity underlies the increase in $GABA_AR$ lateral diffusion in the absence of IICR.

The observation that the loss of IICR revealed the role of basal calcineurin activity to increase $GABA_AR$ diffusion

(E) Time course of DHPG-induced intracellular Ca^{2+} elevation as reported by measurement of Fluo-4 F/F_0 ratio (means ± SEM; n = 41).

(F and G) Representative images (F) and quantifications (G) of the fluorescence intensity of synaptic $GABA_AR$ clusters showing that DHPG increases $GABA_AR$ clustering. Values (mean ± SEM) were normalized to their respective control values (n ≥ 30 cells per condition; ***$p < 0.005$, *$p < 0.05$, *t*-test). Scale bars, 10 μm. See also Figures S1–S5.

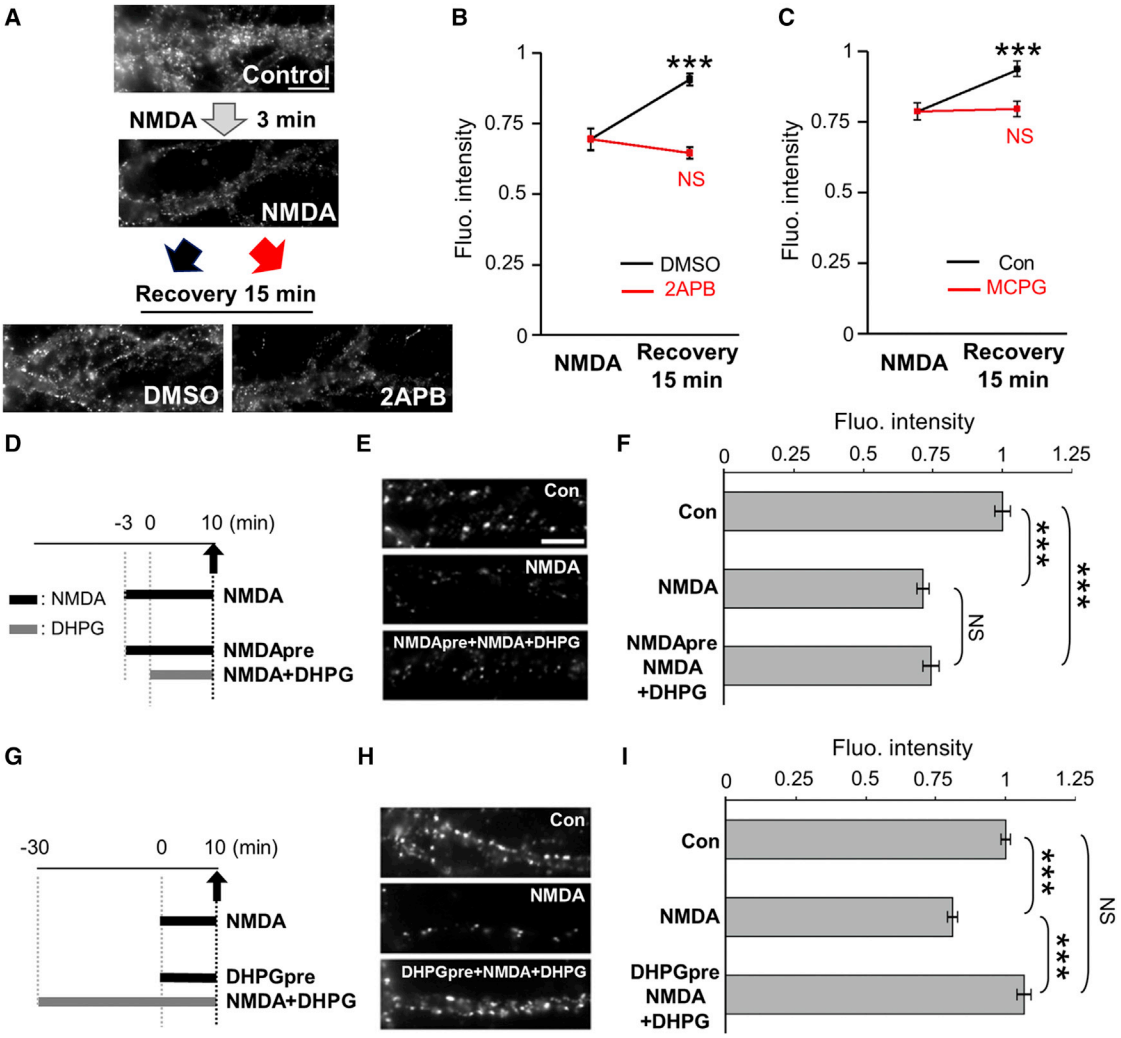

Figure 4. mGluR/IICR Contribute to the Positive Control of $GABA_AR$ Clustering through Separate Non-overlapping Mechanisms with Ca^{2+} Influx

(A–C) Inhibition of IICR prevents re-clustering of $GABA_AR$ at synapses after NMDA washout. (A) Examples show $GABA_AR$ γ2 immunoreactivities after 3-min exposure to NMDA (top) or after 15 min of NMDA washout in the presence of DMSO (middle) or 2APB (bottom). Scale bar, 10 μm. (B and C) Quantification of the fluorescence intensity of $GABA_AR\gamma2$ before (NMDA) and after washout (Recovery), in the presence or absence of 2APB (B) or MCPG (C), is shown. Values (mean ± SEM) were normalized to their respective control values (n = 30 cells/condition; ***$p < 0.005$, *t*-test).

(D–I) Pre-activation of IICR prevents NMDA-mediated dispersion of $GABA_AR$. Neurons pre-incubated to NMDA (D–F) or DHPG (G–I) were then exposed to NMDA in the presence of DHPG. Images (E and H) and quantifications of synaptic cluster fluorescence intensities (F and I) reveal that DHPG restored $GABA_AR$ clustering only when neurons were pre-treated with DHPG. Scale bars, 10 μm. Values (mean ± SEM) were normalized to their respective control values (n = 30–60 cells per condition; ***$p < 0.005$, Tukey's range test in ANOVA).

suggested the possibility that IICR physiologically activates a phosphorylation pathway antagonizing the de-phosphorylation effect of calcineurin to reduce $GABA_AR$ diffusion. Because conventional α, β, and γ subtypes of protein kinase C (PKC) are activated by Ca^{2+} and diacylglycerol (DAG) downstream of mGluR1/5, we hypothesized that IICR reduces lateral diffusion of $GABA_AR$ following PKC-dependent phosphorylation of target proteins. Therefore, we examined the effect of 2APB treatment on the expression level and the intracellular distribution of Ca^{2+}-dependent PKCs in cultured hippocampal neurons by western blot and immunocytochemistry, respectively. Western blot analysis revealed that 2APB exposure for 60 min dramatically decreased the expression level of PKCγ to 68.9% ± 6.0% of the control (DMSO), while the expression of PKCα and β2 remained unchanged (PKCα: 94.4% ± 5.6%; PKCβ2: 95.7% ± 4.4%; Figures 6A and 6B). Since there is a possibility that the distribution of protein can change without affecting the total amount of protein, we then quantified the amount of Ca^{2+}-dependent PKCs around surface $GABA_ARs$ using immunocytochemistry (Figure 6C). To estimate the amount of PKCs around surface $GABA_ARs$, we measured the mean PKC fluorescence intensity per pixel overlapping

with $GABA_AR$ clusters. Although the fluorescence intensity beneath $GABA_AR$ clusters of PKCα was unaffected (PKCα: 97.0% ± 1.8%; Figure 6D), that of PKCβ2 and γ significantly decreased after 2APB treatment (PKCβ2: 91.8% ± 1.1%; PKCγ: 81.9% ± 1.6%; Figure 6D). We concluded that the IICR pathway regulates the expression level and subcellular distribution of PKCs.

We reasoned that if IICR constrains the diffusion of $GABA_AR$ through PKC-dependent phosphorylation, the blockade of PKC should mimic the effect of the IICR inhibitor 2APB. Indeed, neurons exposed to 12-(2-cyanoethyl)-6,7,12,13-tetrahydro-13-methyl-5-oxo-5H-indolo(2,3-a)pyrrolo(3,4-c)-carbazole (Gö6976), a specific inhibitor against PKCα, β, and γ (Keenan et al., 1997; Martiny-Baron et al., 1993), for 60–90 min (500 nM; Figure 7A) had an increased diffusion coefficient (Figures 7B and 7C), reduced synaptic dwell time (Figure 7D), and enlarged confinement size (Figure 7E). This behavior is reminiscent of the effect of 2APB on $GABA_AR$ diffusion (Figure 5). In turn, the PKC activator phorbol 12-myristate 13-acetate (PMA, 200 nM), which mimics DAG, but not its inactive analog 4α-phorbol 12-myristate 13-acetate (4α-PMA) (Figure 7A), abolished the 2APB effect on $GABA_AR$ mobility (Figure 7F–7I).

Dephosphorylation of Serine 327 of the $GABA_AR$ γ2 subunit (S327) by calcineurin has been reported to enhance the lateral diffusion of $GABA_AR$ (Muir et al., 2010). Interestingly, S327 is also a PKC target (Moss et al., 1992). Therefore, we examined whether IICR-mediated regulation of $GABA_AR$ mobility relies on the phosphorylation of S327 by mutating S327 to alanine (S327A) or glutamate (S327E) to mimic the dephosphorylated and phosphorylated forms of the receptor, respectively (Figure S7A). A myc-tag was added to the N-terminal region of the chimera in order to track the mutant receptor with QD-coupled myc-tag antibodies. We found 2APB significantly enhanced the diffusion of S327A and S327E chimeras similar to the WT $GABA_AR$ (Figure S7B), indicating that S327 is not involved in the 2APB effect. S343, an additional potential PKC target in $GABA_AR$γ2L (Moss et al., 1992), was mutated in concert with S327 to alanine (S327/343A) or glutamate (S327/343E). However, neither S327/343A nor S327/343E prevented the 2APB-induced increase in $GABA_AR$ diffusion (Figure S7C), suggesting that IICR-dependent regulation of $GABA_AR$ mobility does not require S327 or S343 of the $GABA_AR$γ2 subunit, but involves other PKC target residues.

Altogether these results implicate PKC activation and, therefore, increased phosphorylation of target protein(s) in the IICR-induced constrain of $GABA_AR$ lateral diffusion. In the hippocampal neurons, the second messenger Ca^{2+} has a dualistic impact on $GABA_AR$, i.e., intracellular Ca^{2+} elevation has opposite effects on the regulation of $GABA_AR$ lateral diffusion and clustering. Ca^{2+} influx through NMDAR activates calcineurin, leading to an increase of $GABA_AR$ lateral diffusion and synaptic escape of the receptor (Bannai et al., 2009; Muir et al., 2010; Figure 7J). In contrast, Ca^{2+} release from the ER stores following mGluR, PLC, and IP_3R activation antagonizes calcineurin activity while activating PKC, which leads to phosphorylation of unknown target(s) and synaptic stabilization of $GABA_ARs$ (Figure 7J).

DISCUSSION

In this study, we demonstrate that the mGluR/IICR/PKC pathway stabilizes GABAergic synapses by constraining lateral diffusion and increasing clustering of $GABA_ARs$, without affecting the total number of $GABA_AR$ on the cell surface. This pathway defines a unique form of homeostatic regulation of GABAergic transmission under conditions of basal synaptic activity and during recovery from E/I imbalances. The study also highlights the ability of neurons to convert a single neurotransmitter (glutamate) into an asymmetric control system for synaptic efficacy using different calcium-signaling pathways.

In hippocampal neurons, GABAergic synapses have two regulatory mechanisms as follows: a plastic regulation of $GABA_AR$ clustering by Ca^{2+} influx through NMDARs (Bannai et al., 2009; Luscher et al., 2011; Marsden et al., 2010; Muir et al., 2010; Petrini et al., 2014), and a homeostatic stabilization process that contributes to the continuous maintenance of GABAergic synapse structure and the recovery from anti-homeostatic destabilization. Our results provide further insight into this second system, showing that the recovery of synaptic $GABA_AR$ clusters from NMDA-induced dispersal is impaired when IP_3R and mGluR signaling are inhibited. These findings support the idea that continuous IICR activity downstream of mGluRs plays a crucial role in recovery from the transient decrease in synaptic $GABA_AR$ numbers accompanying excess neuronal activity and the stabilization of GABAergic synapses under both normal and pathological conditions.

Our data raise the possibility that mGluR-dependent IICR contributes to the maintenance of GABAergic synapses under physiological conditions. Gene KO of IP_3R1 or pharmacological inhibition of IICR led to a reduction of synaptic $GABA_AR$ numbers and mIPSC amplitude, indicating that the constitutive IICR activity is involved in the maintenance of GABAergic synapses. Considering that group I mGluRs are tonically activated by ambient glutamate (Smolders et al., 2004), mGluR-dependent IICR could occur in a constitutive manner under basal conditions to maintain the integrity of GABAergic synapses.

Our findings also suggest a possible role of constitutive IICR in synaptic plasticity. Although several alterations of synaptic plasticity have been reported in IP_3R1KO hippocampal neurons such as LTD-LTP conversion (Nishiyama et al., 2000) and LTP facilitation in excitatory synapses (Fujii et al., 2000; Itoh et al., 2001), the mechanisms underlying these modifications mostly remain unknown. LTP facilitation in IP_3R1KO hippocampus CA1 is due to weakened inhibitory input (Yoshioka et al., 2010), and this could be explained by our finding that loss of mGluR or IICR impaired GABAergic synaptic transmission through enhanced synaptic escape of $GABA_AR$ by diffusion. In other words, mGluR/IICR signaling could ensure physiological LTP by restoring post-plasticity stabilization of GABAergic synapses that would have a tonic effect on the physiological set point for network stability.

The most striking conceptual finding in this study is that two distinct intracellular signaling pathways, NMDAR-driven Ca^{2+} influx and mGluR-driven Ca^{2+} release from the ER, effectively driven by the same neurotransmitter, glutamate, have an opposing impact on the stability and function of GABAergic synapses. Sustained Ca^{2+} influx through ionotropic glutamate

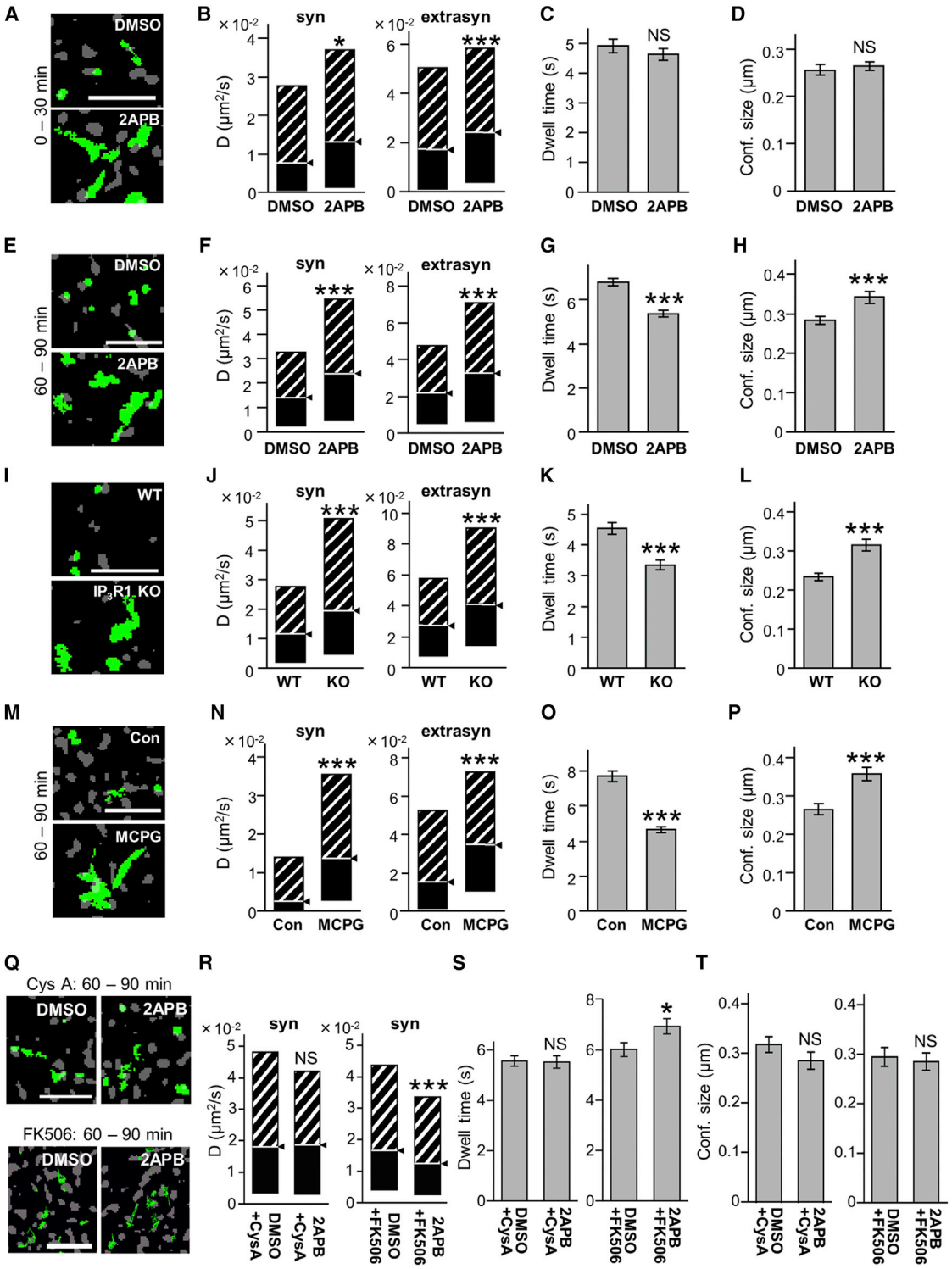

Figure 5. Reduced IICR Activity Increases the Lateral Diffusion of $GABA_AR$ γ2 Subunits in the Presence of Calcineurin Activity

QD-SPT tracking of $GABA_AR$ γ2 subunits in hippocampal neurons. (A, E, I, M, and Q) Examples show QD trajectories (green), reconstructed from recording sequences (15.2 s for I and 38.4 s for others), overlaid with FM4-64 signals (gray) in order to identify synapses. Scale bars, 5 μm. (B, F, J, N, and R) Quantifications of median diffusion coefficients are shown (median D ± 25%–75% Interquartile Range [IQR]). (C, G, K, O, and S) The mean (±SEM) synaptic dwell time is shown. (D, H, L, P, and T) Size of confinement domains is shown (mean ± SEM).

(legend continued on next page)

receptor-dependent calcium signaling increases $GABA_AR$ lateral diffusion, thereby causing the dispersal of synaptic $GABA_AR$, while tonic mGluR-mediated IICR restrains the diffusion of $GABA_AR$, thus increasing its synaptic density. How can Ca^{2+} influx and IICR exert opposing effects on GABA synaptic structure? Our research indicates that each Ca^{2+} source activates a different Ca^{2+}-dependent phosphatase/kinase: NMDAR-dependent Ca^{2+} influx activates calcineurin, while ER Ca^{2+} release activates PKC.

We found that the increased lateral diffusion of $GABA_AR$ was attenuated by the inhibition of calcineurin, which remains active even at basal levels of Ca^{2+} concentration (Nabavi et al., 2013). This implies that $GABA_AR$ lateral diffusion could be under the control of calcineurin not only after Ca^{2+} influx, when neuronal excitation is enhanced, but also during basal levels of activity. Moreover, the enhancement of $GABA_AR$ diffusion by PKC inhibition indicates that PKC is also normally active under basal conditions. Active PKCs translocate to the plasma membrane (Newton, 1997). Therefore, the fact that 2APB decreased the amount of PKC-β2 and -γ colocalizing with $GABA_AR$ clusters suggests that constitutive activation of the IICR pathway may maintain the expression and activity of PKC.

It is noteworthy that the impact of a PKC inhibitor alone on $GABA_AR$ diffusion was more prominent than that of a calcineurin inhibitor alone under basal conditions, suggesting that constitutive PKC activity for synaptic stability overcomes basal calcineurin activity in neurons with a physiological E/I balance. However, the mechanism of how PKC phosphorylation impacts $GABA_AR$ diffusion remains to be elucidated in future study. $GABA_AR$ scaffold-binding affinity could be regulated by PKC. Considering that $GABA_AR$ antibody cross-linking prevented the dispersion of gephyrin clusters by 2APB, the possibility of a phosphorylation-dependent regulation of $GABA_AR$ lateral diffusion is independent of the receptor-gephyrin binding control. This implies the involvement of other $GABA_AR$-interacting and -clustering protein(s) (Luscher et al., 2011; Smith et al., 2014). It is also noteworthy that the $GABA_AR\gamma2$ S327 and S343 residues both targeted by PKC are not involved in IICR-mediated regulation of $GABA_AR$ lateral mobility. This contrasts with the fact that calcineurin enhances $GABA_AR$ lateral diffusion via a mechanism involving S327 dephosphorylation (Muir et al., 2010). This suggests that calcineurin and PKC tune $GABA_AR$ mobility by regulation of the phosphorylation state of distinct residues. Furthermore, PKC may affect $GABA_AR$ stability by also controlling the phosphorylation of scaffold molecules.

Taken together, these results lead us to propose the following model for bidirectional competitive regulation of GABAergic synapses by glutamate signaling. Phasic Ca^{2+} influx through NMDARs following sustained neuronal excitation or injury leads to the activation of calcineurin, overcoming PKC activity and relieving $GABA_AR$ diffusion constraints. In contrast, during the maintenance of GABAergic synaptic structures or the recovery from $GABA_AR$ dispersal, the ambient tonic mGluR/IICR pathway constrains $GABA_AR$ diffusion by PKC activity, overcoming basal calcineurin activity. One possible mechanism of dual regulation of $GABA_AR$ by Ca^{2+} is that each Ca^{2+}-dependent enzyme has a unique sensitivity to the frequency and number of external glutamate release events and can act to decode neuronal inputs (Fujii et al., 2013; Li et al., 2012; Stefan et al., 2008) in inhibitory synapses.

Tight control of E/I balance, the loss of which results in epilepsy and other brain and nervous system diseases/disorders, is dependent on GABAergic synaptic transmission (Mann and Paulsen, 2007). A recent study showed that the excitation-induced acceleration of $GABA_AR$ diffusion and subsequent dispersal of $GABA_ARs$ from synapses is the cause of generalized epilepsy febrile seizure plus (GEFS+) syndrome (Bouthour et al., 2012). Our results indicate that pre-activation of the mGluR/IICR pathway by DHPG could completely prevent the dispersion of synaptic $GABA_ARs$ induced by massive excitatory input similar to status epilepticus. Thus, further study of the molecular mechanisms underlying the mGluR/IICR-dependent stabilization of GABAergic synapses via regulation of $GABA_AR$ lateral diffusion and synaptic transmission could be helpful in the prevention or treatment of pathological E/I imbalances, for example, in the recovery of GABAergic synapses from epileptic states.

EXPERIMENTAL PROCEDURES

Animals

All experiments in this study were carried out in accordance with the guidelines approved by the Animal Experiment Committee of the RIKEN and Nagoya Univ.

Primary Cultures of Hippocampal Neurons

Primary cultures of hippocampal neurons were prepared from embryonic day (E)18–E21 Wistar rat embryos or P0–P1 IP_3R1 KO mice (Matsumoto et al., 1996) or their littermates, as previously described (Goslin et al., 1998), and they were used for each experiment at 21–27 days in vitro (DIV), unless otherwise described.

Drug Treatment

Neurons were acutely exposed to the different drugs for the indicated duration at 37°C in imaging medium comprising MEM without phenol red (Life Technologies), 20 mM HEPES, 33 mM glucose, 2 mM glutamine, 1 mM sodium pyruvate, and MACS NeuroBrew-21 (Miltenyi Biotec).

Immunocytochemistry and Quantitative Analysis

Immunochemical detections of $GABA_AR$, gephyrin, synapsin, and PKC in cultured neurons were performed as previously described (Bannai et al., 2009; Niwa et al., 2012) using the following antibodies: rabbit anti-$GABA_AR$ γ2 subunit antibody (Niwa et al., 2012); mouse anti-gephyrin monoclonal

(A–H) Tracking of QD-bound $GABA_AR\gamma2$ subunits in neurons exposed to IP_3R blocker 2APB for 0–30 (A–D) or 60–90 (E–H) min. Note that exploration and diffusion coefficient of $GABA_AR$ increased after 2APB application (A, B, E, and F). In contrast, the mean synaptic dwell time (C and G) and size of confinement domains (D and H) decreased and increased, respectively, only after 60 min, but not before 30 min of drug treatment.
(I–L) Increased diffusion and reduced synaptic confinement in IP_3R1KO neurons (KO) compared with WT, analyzed at 15–18 DIV.
(M–P) The blockade of group I mGluRs also led to an increase in diffusion of $GABA_AR$.
(Q–T) Neurons were exposed to 2APB in the absence or presence of the calcineurin inhibitor Cyclosporin A (CysA) and FK506. Both CysA and FK506 prevented the 2APB-dependent increase in $GABA_AR$ diffusion.
NS, $p > 0.05$; *$p < 0.05$, **$p < 0.01$, ***$p < 0.005$; Mann-Whitney *U*-test (B, F, J, N, and R) and Welch's *t*-test for others. Numbers of QDs analyzed are shown in Table S1. See also Figures S5 and S6.

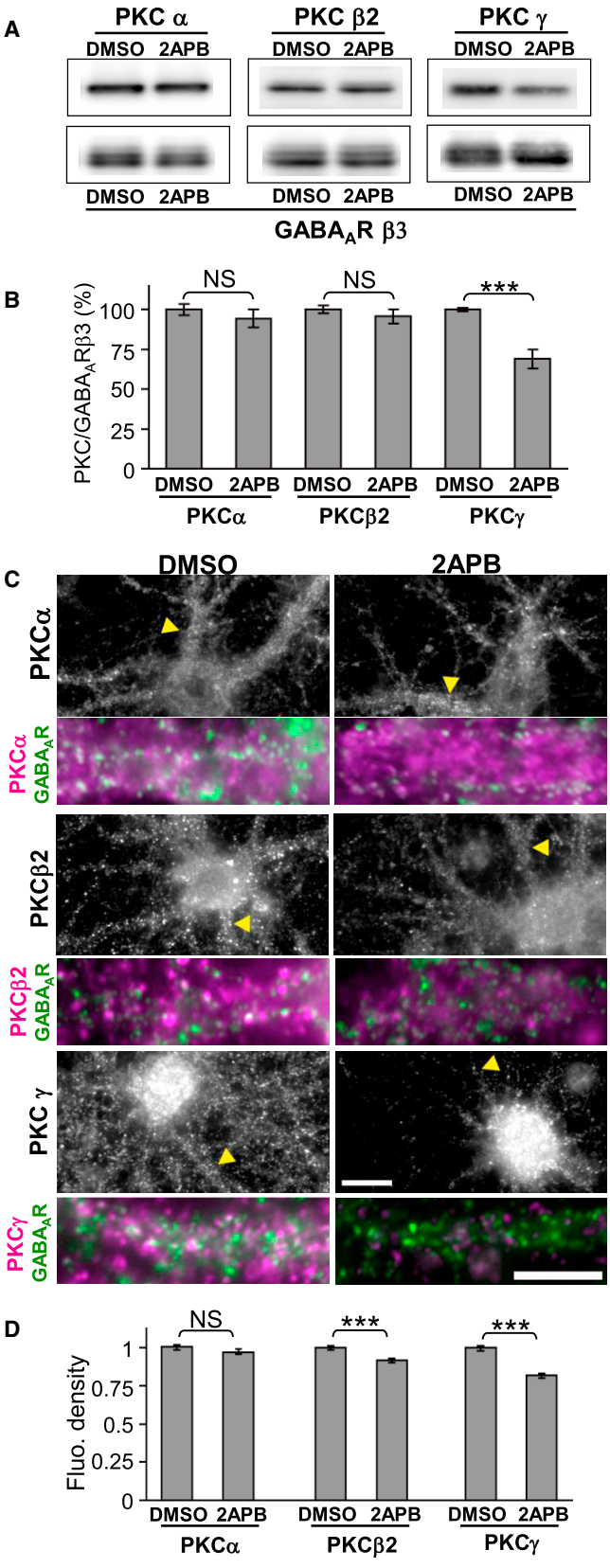

antibody mAb7a (0.33 μg/ml, Synaptic Systems); mouse anti-synapsin I antibody (1:3,000, Synaptic Systems); rabbit polyclonal anti-synapsin I antibody (1:400, Merck Millipore); guinea pig anti-PKCα antibody (1 μg/ml, Frontier Institute); guinea pig anti-PKCβII antibody (1 μg/ml, Frontier Institute); and guinea pig anti-PKCγ antibody (1 μg/ml, Frontier Institute). Images were acquired on an inverted microscope equipped with oil-immersion objectives (60×, numerical aperture [NA] 1.42) and a cooled charge-coupled device (CCD) camera. All images from the same culture were acquired with the same sub-saturation exposure time. Quantification of the fluorescence signal was performed using MetaMorph software (Molecular Devices) as previously described (Bannai et al., 2009; Charrier et al., 2006; Lévi et al., 2004, 2008; Niwa et al., 2012).

Electrophysiology

Whole-cell patch-clamp experiments on primary cultured neurons were carried out with solutions. The internal solution contained the following (in mM): $CsCl_2$, 140; EGTA, 0.2; HEPES, 10; Mg-ATP, 2; GTP-Tris, 1; and Na-phosphocreatine, 2.5 (pH 7.2–7.3, 280–290 mOsm). The extracellular recording solution contained the following (in mM): NaCl, 147; KCl, 2.1; HEPES, 8.8; D-glucose, 8.8; $CaCl_2$, 1.1; $MgCl_2$, 1.1; and Pyruvic Acid, 0.026% (v/v) (pH 7.4, 310 mOsm).

For experiments on acute slice, hippocampal brain slices were prepared from P14–P21 BL56/J IP3R1−/− mice and WT littermates. The internal solution contained the following (in mM): $CsCl_2$, 130; EGTA, 10; $CaCl_2$, 1; $MgCl_2$, 1; HEPES, 10; Mg-ATP, 2; GTP-Tris, 0.1; and Na-phosphocreatine, 2.5 (pH 7.4, 290–300 mOsm). The extracellular recording solution was the artificial cerebrospinal fluid (aCSF) solution and contained the following (in mM): NaCl, 125; KCl, 2.5; D-Glucose, 25; $CaCl_2$, 2; $MgCl_2$, 1; NaH_2PO_4, 1.25; and $NaHCO_3$, 25 (320 mOsm).

Spontaneous mIPSCs were recorded in the whole-cell voltage-clamp configuration, in the presence of 2,3-Dihydroxy-6-nitrobenzo[f]quinoxaline-7-sulfonamide (NBQX, 10 μM), D-2-Amino-5-phosphonopentanoic acid (D-AP5, 50 μM), and TTX (1 μM). When required the extracellular recording solution was supplemented with 250 μM MCPG or vehicle (NaOH). The resistance of whole-cell patch pipettes was 3–5 MΩ. All experiments were performed at room temperature. The membrane potential was held at −70 mV. Under these recording conditions, GABAergic chloride currents were recorded as inward currents.

Production of a Rabbit $GABA_AR$ β3 Subunit Antiserum

The rabbit anti-$GABA_AR$ β3 subunit antiserum (anti-$GABA_AR$ β3) was raised as described previously (Todd et al., 1996). For the sub-cloning of fusion protein consisting of maltose-binding protein (MBP) and amino acids 345–408 of the mouse $GABA_AR$ β3, the DNA sequence corresponding to amino acid 345–408 of the $GABA_AR$ β3 was amplified by PCR, using FANTOM3 clone C630014N19 (RIKEN Genomic Sciences Research Complex) as a template (Carninci et al., 2005), and sub-cloned into pMAL-C vector (New England Biolabs).

Figure 6. IICR Activity Regulates the Expression Level and Clustering of Ca^{2+}-Dependent PKC

(A) Protein expression levels of α, β2, and γ PKC subtypes and $GABA_AR$ β3 subunit after 60-min exposure of neurons to DMSO or 2APB are shown.

(B) Quantification of the PKC/$GABA_AR$ β3 subunit protein level ratio showing the PKCγ/$GABA_AR$ β3 ratio significantly decreased after 2APB exposure for 60 min. Values (mean ± SEM) were normalized to the respective DMSO control condition (n = 6; ***p < 0.005, *t*-test).

(C) Co-staining of $GABA_AR$ γ2 subunit and α, β2, or γ PKC subtypes after 60 min of DMSO or 2APB treatment. Arrowheads in upper panels indicate the dendrites enlarged in lower panels. Color codes in lower panels are as follows: green, $GABA_AR$; magenta, α, β2, or γ PKC; and white, $GABA_AR$ and PKC colocalized clusters. Scale bars, 10 μm. Note that 2APB decreased the PKC β2 and γ, but not α, isoform immunoreactivities.

(D) PKC fluorescence intensity per pixel below $GABA_AR$ punctae. Values (mean ± SEM) were normalized to the respective DMSO control condition (n = 30 cells for PKCα and PKCβ2; n = 40 for PKCγ; ***p < 0.005, *t*-test).

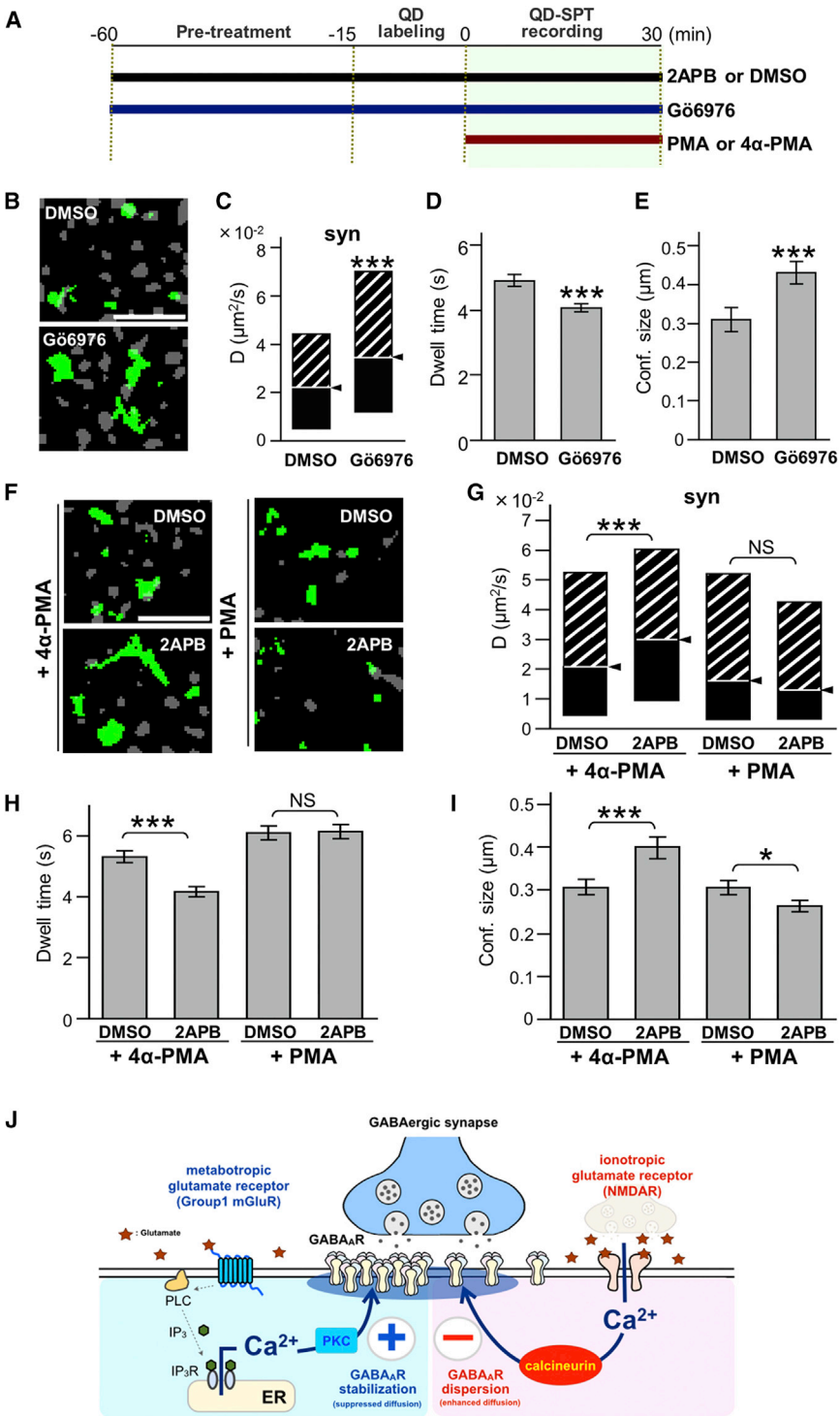

Figure 7. Constraint of $GABA_AR$ Lateral Diffusion Requires Ca^{2+}-Dependent PKC Activity

(A) A diagram showing the time course of the experiment. Drugs were applied as indicated by horizontal bars.

(B–E) Blockade of Ca^{2+}-dependent PKC by Gö6976 (60–90 min) enhances $GABA_AR$ surface exploration (B, green), diffusion coefficients (C, median D values ± IQR), synaptic escape (D, mean dwell time ± SEM), and size of confinement domain (E, mean ± SEM).

(F–I) The PKC activator PMA, but not its inactive form (4α-PMA), prevented the 2APB-induced enhancement of $GABA_AR$ mobility (***$p < 0.005$; NS, $p > 0.05$; Mann-Whitney *U*-test (C and G) and Welch's *t*-test (D, E, H, and I). Numbers of QDs analyzed are shown in Table S1. Scale bars, 5 μm (A and E).

(J) Conceptual diagrams showing summary of our finding. Massive Ca^{2+} influx through NMDAR activates calcineurin (CN), exceeds phosphorylation by PKC, and results in increasing lateral diffusion of $GABA_AR$ on the plasma membrane (PM). In contrast, the mGluR/PLC/IICR pathway constitutively activates PKC. This activation of mGluR/IICR/PKC process constrains lateral diffusion of $GABA_AR$, counteracting basal activity of CN.

See also Figure S7.

Western Blot

For western blot analysis, the following primary antibodies were used: rabbit anti-$GABA_AR$ β3 antiserum (1:2,000); rabbit anti-PKCα antiserum (1:100,000, Sigma-Aldrich); guinea pig anti-PKCβII antibody (200 ng/ml, Frontier Institute); or guinea pig anti-PKCγ antibody (200 ng/ml, Frontier Institute). The primary antibodies were recognized using horseradish peroxidase (HRP)-coupled goat anti-rabbit IgG (1:5,000, GE Healthcare) or goat anti-guinea pig IgG (1:5,000, Cappel). Chemiluminescence from HRP reacted to Immobilon Western Chemiluminescent HRP Substrate (Merck Millipore) was detected by Imagequant LAS-4000 mini (GE Healthcare) and quantified using ImageJ.

Ca^{2+} Imaging

Ca^{2+} imaging was performed as described previously (Bannai et al., 2009; Niwa et al., 2012). Neurons were incubated with 0.5 μM fluo-4 AM (Life Technologies) and fluo-4 signal was acquired at 0.2 Hz at room temperature (24°C–26°C). The ratio of the fluorescence intensities F/F0, where F is a fluorescence intensity and F0 is the intensity at t = 0, was obtained after subtraction of the background fluorescence.

QD-SPT Experiments and Data Analysis

QD labeling and SPT of $GABA_ARs$ were performed as previously described (Bannai et al., 2006). Rabbit anti-$GABA_AR\gamma2$ antibody (2.0 μg/ml; Niwa et al., 2012) was used for the labeling of $GABA_AR$. Recording was performed at 37°C in the imaging medium using an inverted microscope (IX-70, -71, or -73, Olympus) equipped with an oil-immersion objective (60×, NA > 1.42, Olympus) and a cooled CCD camera (ORCA-II-ER, Hamamatsu Photonics) or an EM-CCD camera (Cascade, Roper Scientific; ImagEM, Hamamatsu Photonics). Fluorescent signals were detected using appropriate filter sets for QD (excitation: 455 ± 70 nm, emission: 605 ± 20 nm) and FM4-64 (excitation: 535 ± 15 nm, emission: 580 nm long pass). QD movies were recorded with an integration time of 76 ms with 512 consecutive frames (38.9 s) or 200 frames for IP_3R1KO neurons. All recordings were finished within 30 min after labeling. QD-SPD data were analyzed using TI workbench

software written by Dr. T. Inoue (Waseda University) as described previously (Bannai et al., 2009; Niwa et al., 2012).

Details of other methods are presented in the Supplemental Experimental Procedures.

SUPPLEMENTAL INFORMATION

Supplemental Information includes Supplemental Experimental Procedures, seven figures, and one table and can be found with this article online at http://dx.doi.org/10.1016/j.celrep.2015.12.002.

AUTHOR CONTRIBUTIONS

H.B. and F.N. developed the concept, designed and performed the experiments, analyzed data, and wrote the paper. M.W.S., A.N.S., M.A., A.M., and K.S. performed experiments and analyzed data. S.L. developed SPT and immunocytochemistry, provided conceptual advice, and wrote the paper. A.T. and K.M. supervised the whole project.

ACKNOWLEDGMENTS

We thank the Research Resource Center (RIKEN BSI) for FANTOM3 clone and for supporting antibody production. We thank C. Hisatsune and S. Sakuragi for technical supports; T. Inoue, M. Dahan, V. Racine, and J.B. Sibarita for the analysis program; and Y. Oda, I. Mori, C. Yokoyama, and A.V. Terashima for their valuable comments on the manuscript. This work was supported by RIKEN (Special Postdoctoral Researcher [SPDR] and Foreign Postdoctoral Researcher [FPR] programs); KAKENHI (20700300, 25830058, 20220007, and "Glial assembly" 26117509); Japan Society for the Promotion of Science (JSPS, 06J06775); research grants from the Toyobo Biotechnology Foundation, Kato Memorial Bioscience Foundation, and Toray Science Foundation; and the Moritani Scholarship Foundation. Work in the A.T. laboratory was supported by the European Research Council (ERC) grant PlastInhib and the L'Agence Nationale de la Recherche (ANR) grant Synaptune, The Labex Memolife (ANR-10-LABX-54) and PSL Research University (ANR-11-IDEX-0001-02). We thank two anonymous reviewers for their insightful and constructive comments on the manuscript.

Received: January 13, 2015
Revised: August 13, 2015
Accepted: November 19, 2015
Published: December 17, 2015

REFERENCES

Bannai, H., Lévi, S., Schweizer, C., Dahan, M., and Triller, A. (2006). Imaging the lateral diffusion of membrane molecules with quantum dots. Nat. Protoc. *1*, 2628–2634.

Bannai, H., Lévi, S., Schweizer, C., Inoue, T., Launey, T., Racine, V., Sibarita, J.B., Mikoshiba, K., and Triller, A. (2009). Activity-dependent tuning of inhibitory neurotransmission based on GABAAR diffusion dynamics. Neuron *62*, 670–682.

Berridge, M.J. (1998). Neuronal calcium signaling. Neuron *21*, 13–26.

Bouthour, W., Leroy, F., Emmanuelli, C., Carnaud, M., Dahan, M., Poncer, J.C., and Lévi, S. (2012). A human mutation in Gabrg2 associated with generalized epilepsy alters the membrane dynamics of GABAA receptors. Cereb. Cortex *22*, 1542–1553.

Calamai, M., Specht, C.G., Heller, J., Alcor, D., Machado, P., Vannier, C., and Triller, A. (2009). Gephyrin oligomerization controls GlyR mobility and synaptic clustering. J. Neurosci. *29*, 7639–7648.

Carninci, P., Kasukawa, T., Katayama, S., Gough, J., Frith, M.C., Maeda, N., Oyama, R., Ravasi, T., Lenhard, B., Wells, C., et al.; FANTOM Consortium; RIKEN Genome Exploration Research Group and Genome Science Group (Genome Network Project Core Group) (2005). The transcriptional landscape of the mammalian genome. Science *309*, 1559–1563.

Charrier, C., Ehrensperger, M.V., Dahan, M., Lévi, S., and Triller, A. (2006). Cytoskeleton regulation of glycine receptor number at synapses and diffusion in the plasma membrane. J. Neurosci. *26*, 8502–8511.

Choquet, D., and Triller, A. (2013). The dynamic synapse. Neuron *80*, 691–703.

Eichler, S.A., and Meier, J.C. (2008). E-I balance and human diseases - from molecules to networking. Front. Mol. Neurosci. *1*, 2.

Fujii, S., Matsumoto, M., Igarashi, K., Kato, H., and Mikoshiba, K. (2000). Synaptic plasticity in hippocampal CA1 neurons of mice lacking type 1 inositol-1,4,5-trisphosphate receptors. Learn. Mem. *7*, 312–320.

Fujii, H., Inoue, M., Okuno, H., Sano, Y., Takemoto-Kimura, S., Kitamura, K., Kano, M., and Bito, H. (2013). Nonlinear decoding and asymmetric representation of neuronal input information by CaMKIIα and calcineurin. Cell Rep. *3*, 978–987.

Furuichi, T., Simon-Chazottes, D., Fujino, I., Yamada, N., Hasegawa, M., Miyawaki, A., Yoshikawa, S., Guénet, J.L., and Mikoshiba, K. (1993). Widespread expression of inositol 1,4,5-trisphosphate receptor type 1 gene (Insp3r1) in the mouse central nervous system. Receptors Channels *1*, 11–24.

Gaiarsa, J.L., Caillard, O., and Ben-Ari, Y. (2002). Long-term plasticity at GABAergic and glycinergic synapses: mechanisms and functional significance. Trends Neurosci. *25*, 564–570.

Gerrow, K., and Triller, A. (2010). Synaptic stability and plasticity in a floating world. Curr. Opin. Neurobiol. *20*, 631–639.

Goslin, K., Asmussen, H., and Banker, G. (1998). Rat hippocampal neurons in low-density culture. In Culturing nerve cells, G. Banker and K. Goslin, eds. (Cambridge: MIT press), pp. 339–370.

Haider, B., Duque, A., Hasenstaub, A.R., and McCormick, D.A. (2006). Neocortical network activity in vivo is generated through a dynamic balance of excitation and inhibition. J. Neurosci. *26*, 4535–4545.

Hensch, T.K. (2004). Critical period regulation. Annu. Rev. Neurosci. *27*, 549–579.

Hisatsune, C., Kuroda, Y., Akagi, T., Torashima, T., Hirai, H., Hashikawa, T., Inoue, T., and Mikoshiba, K. (2006). Inositol 1,4,5-trisphosphate receptor type 1 in granule cells, not in Purkinje cells, regulates the dendritic morphology of Purkinje cells through brain-derived neurotrophic factor production. J. Neurosci. *26*, 10916–10924.

Hisatsune, C., Miyamoto, H., Hirono, M., Yamaguchi, N., Sugawara, T., Ogawa, N., Ebisui, E., Ohshima, T., Yamada, M., Hensch, T.K., et al. (2013). IP3R1 deficiency in the cerebellum/brainstem causes basal ganglia-independent dystonia by triggering tonic Purkinje cell firings in mice. Front. Neural Circuits *7*, 156.

Itoh, S., Ito, K., Fujii, S., Kaneko, K., Kato, K., Mikoshiba, K., and Kato, H. (2001). Neuronal plasticity in hippocampal mossy fiber-CA3 synapses of mice lacking the inositol-1,4,5-trisphosphate type 1 receptor. Brain Res. *901*, 237–246.

Jovanovic, J.N., Thomas, P., Kittler, J.T., Smart, T.G., and Moss, S.J. (2004). Brain-derived neurotrophic factor modulates fast synaptic inhibition by regulating GABA(A) receptor phosphorylation, activity, and cell-surface stability. J. Neurosci. *24*, 522–530.

Keenan, C., Goode, N., and Pears, C. (1997). Isoform specificity of activators and inhibitors of protein kinase C gamma and delta. FEBS Lett. *415*, 101–108.

Kilman, V., van Rossum, M.C., and Turrigiano, G.G. (2002). Activity deprivation reduces miniature IPSC amplitude by decreasing the number of postsynaptic GABA(A) receptors clustered at neocortical synapses. J. Neurosci. *22*, 1328–1337.

Kittler, J.T., Thomas, P., Tretter, V., Bogdanov, Y.D., Haucke, V., Smart, T.G., and Moss, S.J. (2004). Huntingtin-associated protein 1 regulates inhibitory synaptic transmission by modulating gamma-aminobutyric acid type A receptor membrane trafficking. Proc. Natl. Acad. Sci. USA *101*, 12736–12741.

Kittler, J.T., Chen, G., Kukhtina, V., Vahedi-Faridi, A., Gu, Z., Tretter, V., Smith, K.R., McAinsh, K., Arancibia-Carcamo, I.L., Saenger, W., et al. (2008). Regulation of synaptic inhibition by phospho-dependent binding of the AP2 complex to a YECL motif in the GABAA receptor gamma2 subunit. Proc. Natl. Acad. Sci. USA *105*, 3616–3621.

Lévi, S., Logan, S.M., Tovar, K.R., and Craig, A.M. (2004). Gephyrin is critical for glycine receptor clustering but not for the formation of functional GABAergic synapses in hippocampal neurons. J. Neurosci. *24*, 207–217.

Lévi, S., Schweizer, C., Bannai, H., Pascual, O., Charrier, C., and Triller, A. (2008). Homeostatic regulation of synaptic GlyR numbers driven by lateral diffusion. Neuron *59*, 261–273.

Lévi, S., Dahan, M., and Triller, A. (2011). Labeling neuronal membrane receptors with quantum dots. Cold Spring Harb. Protoc. *2011*, prot5580.

Li, L., Stefan, M.I., and Le Novère, N. (2012). Calcium input frequency, duration and amplitude differentially modulate the relative activation of calcineurin and CaMKII. PLoS ONE *7*, e43810.

Luscher, B., Fuchs, T., and Kilpatrick, C.L. (2011). GABAA receptor trafficking-mediated plasticity of inhibitory synapses. Neuron *70*, 385–409.

Mann, E.O., and Mody, I. (2010). Control of hippocampal gamma oscillation frequency by tonic inhibition and excitation of interneurons. Nat. Neurosci. *13*, 205–212.

Mann, E.O., and Paulsen, O. (2007). Role of GABAergic inhibition in hippocampal network oscillations. Trends Neurosci. *30*, 343–349.

Marsden, K.C., Shemesh, A., Bayer, K.U., and Carroll, R.C. (2010). Selective translocation of Ca2+/calmodulin protein kinase IIalpha (CaMKIIalpha) to inhibitory synapses. Proc. Natl. Acad. Sci. USA *107*, 20559–20564.

Martiny-Baron, G., Kazanietz, M.G., Mischak, H., Blumberg, P.M., Kochs, G., Hug, H., Marmé, D., and Schächtele, C. (1993). Selective inhibition of protein kinase C isozymes by the indolocarbazole Gö 6976. J. Biol. Chem. *268*, 9194–9197.

Maruyama, T., Kanaji, T., Nakade, S., Kanno, T., and Mikoshiba, K. (1997). 2APB, 2-aminoethoxydiphenyl borate, a membrane-penetrable modulator of Ins(1,4,5)P3-induced Ca2+ release. J. Biochem. *122*, 498–505.

Matsumoto, M., Nakagawa, T., Inoue, T., Nagata, E., Tanaka, K., Takano, H., Minowa, O., Kuno, J., Sakakibara, S., Yamada, M., et al. (1996). Ataxia and epileptic seizures in mice lacking type 1 inositol 1,4,5-trisphosphate receptor. Nature *379*, 168–171.

Mikoshiba, K. (2011). Role of IP_3 receptor in development. Cell Calcium *49*, 331–340.

Moss, S.J., Doherty, C.A., and Huganir, R.L. (1992). Identification of the cAMP-dependent protein kinase and protein kinase C phosphorylation sites within the major intracellular domains of the beta 1, gamma 2S, and gamma 2L subunits of the gamma-aminobutyric acid type A receptor. J. Biol. Chem. *267*, 14470–14476.

Muir, J., Arancibia-Carcamo, I.L., MacAskill, A.F., Smith, K.R., Griffin, L.D., and Kittler, J.T. (2010). NMDA receptors regulate GABAA receptor lateral mobility and clustering at inhibitory synapses through serine 327 on the γ2 subunit. Proc. Natl. Acad. Sci. USA *107*, 16679–16684.

Nabavi, S., Kessels, H.W., Alfonso, S., Aow, J., Fox, R., and Malinow, R. (2013). Metabotropic NMDA receptor function is required for NMDA receptor-dependent long-term depression. Proc. Natl. Acad. Sci. USA *110*, 4027–4032.

Newton, A.C. (1997). Regulation of protein kinase C. Curr. Opin. Cell Biol. *9*, 161–167.

Newton, A.J., Kirchhausen, T., and Murthy, V.N. (2006). Inhibition of dynamin completely blocks compensatory synaptic vesicle endocytosis. Proc. Natl. Acad. Sci. USA *103*, 17955–17960.

Nishiyama, M., Hong, K., Mikoshiba, K., Poo, M.M., and Kato, K. (2000). Calcium stores regulate the polarity and input specificity of synaptic modification. Nature *408*, 584–588.

Niwa, F., Bannai, H., Arizono, M., Fukatsu, K., Triller, A., and Mikoshiba, K. (2012). Gephyrin-independent GABA(A)R mobility and clustering during plasticity. PLoS ONE *7*, e36148.

Nusser, Z., Cull-Candy, S., and Farrant, M. (1997). Differences in synaptic GABA(A) receptor number underlie variation in GABA mini amplitude. Neuron *19*, 697–709.

Nusser, Z., Hájos, N., Somogyi, P., and Mody, I. (1998). Increased number of synaptic GABA(A) receptors underlies potentiation at hippocampal inhibitory synapses. Nature *395*, 172–177.

Petrini, E.M., and Barberis, A. (2014). Diffusion dynamics of synaptic molecules during inhibitory postsynaptic plasticity. Front. Cell. Neurosci. *8*, 300.

Petrini, E.M., Ravasenga, T., Hausrat, T.J., Iurilli, G., Olcese, U., Racine, V., Sibarita, J.B., Jacob, T.C., Moss, S.J., Benfenati, F., et al. (2014). Synaptic recruitment of gephyrin regulates surface GABAA receptor dynamics for the expression of inhibitory LTP. Nat. Commun. *5*, 3921.

Sieghart, W., Fuchs, K., Tretter, V., Ebert, V., Jechlinger, M., Höger, H., and Adamiker, D. (1999). Structure and subunit composition of GABA(A) receptors. Neurochem. Int. *34*, 379–385.

Smith, K.R., Davenport, E.C., Wei, J., Li, X., Pathania, M., Vaccaro, V., Yan, Z., and Kittler, J.T. (2014). GIT1 and βPIX are essential for GABA(A) receptor synaptic stability and inhibitory neurotransmission. Cell Rep. *9*, 298–310.

Smolders, I., Lindekens, H., Clinckers, R., Meurs, A., O'Neill, M.J., Lodge, D., Ebinger, G., and Michotte, Y. (2004). In vivo modulation of extracellular hippocampal glutamate and GABA levels and limbic seizures by group I and II metabotropic glutamate receptor ligands. J. Neurochem. *88*, 1068–1077.

Stefan, M.I., Edelstein, S.J., and Le Novère, N. (2008). An allosteric model of calmodulin explains differential activation of PP2B and CaMKII. Proc. Natl. Acad. Sci. USA *105*, 10768–10773.

Sugawara, T., Hisatsune, C., Le, T.D., Hashikawa, T., Hirono, M., Hattori, M., Nagao, S., and Mikoshiba, K. (2013). Type 1 inositol trisphosphate receptor regulates cerebellar circuits by maintaining the spine morphology of purkinje cells in adult mice. J. Neurosci. *33*, 12186–12196.

Takei, K., Shin, R.M., Inoue, T., Kato, K., and Mikoshiba, K. (1998). Regulation of nerve growth mediated by inositol 1,4,5-trisphosphate receptors in growth cones. Science *282*, 1705–1708.

Todd, A.J., Watt, C., Spike, R.C., and Sieghart, W. (1996). Colocalization of GABA, glycine, and their receptors at synapses in the rat spinal cord. J. Neurosci. *16*, 974–982.

Triller, A., and Choquet, D. (2005). Surface trafficking of receptors between synaptic and extrasynaptic membranes: and yet they do move!. Trends Neurosci. *28*, 133–139.

Triller, A., and Choquet, D. (2008). New concepts in synaptic biology derived from single-molecule imaging. Neuron *59*, 359–374.

Yizhar, O., Fenno, L.E., Prigge, M., Schneider, F., Davidson, T.J., O'Shea, D.J., Sohal, V.S., Goshen, I., Finkelstein, J., Paz, J.T., et al. (2011). Neocortical excitation/inhibition balance in information processing and social dysfunction. Nature *477*, 171–178.

Yoshioka, M., Yamazaki, Y., Fujii, S., Kaneko, K., Kato, H., and Mikoshiba, K. (2010). Intracellular calcium ion dynamics involved in long-term potentiation in hippocampal CA1 neurons in mice lacking the IP3 type 1 receptor. Neurosci. Res. *67*, 149–155.

Cell Reports

Supplemental Information

Bidirectional Control of Synaptic $GABA_AR$ Clustering by Glutamate and Calcium

Hiroko Bannai, Fumihiro Niwa, Mark W. Sherwood, Amulya Nidhi Shrivastava, Misa Arizono, Akitoshi Miyamoto, Kotomi Sugiura, Sabine Lévi, Antoine Triller, and Katsuhiko Mikoshiba

1. Supplemental Experimental Procedures

Animals

All experiments in this study were carried out in accordance with the guidelines issued by the Japanese Ministry of Education, Culture, Sports, Science and Technology and approved by the Animal Experiment Committee of the RIKEN and Nagoya Univ. IP_3R1 knock-out mice and Homozygous mRFP-gephyrin knock-in mice are described previously (Calamai et al., 2009; Matsumoto et al., 1996).

Primary cultures of hippocampal neurons

Primary cultures of hippocampal neurons were prepared from E18–21 Wistar rat embryos as previously described (Goslin et al., 1998). Neurons were plated at a density of $1.3x10^4$ cells/cm^2 onto glass coverslips coated with 80 μg/ml poly-D, L-ornithine or 0.04% polyethyleneimine (Sigma). Cultures were maintained in Neurobasal medium supplemented with B27, 2 mM L-glutamine, and antibiotics (all from Life Technologies, CA, USA). Cells were cultured at 37°C in a 5% CO_2. At least three independent cultures were used for each experiment at 21–27 days *in vitro* (DIV) unless described.

Drug treatment

The following drugs were used: 2APB (100 μM; Daiichi Kagaku, Japan) to block IP_3R channel activity, U73122 (1 μM; Calbiochem, CA, USA) to inhibit IP_3 production and MCPG (250 μM; Tocris, MO, USA) to antagonize mGluR activity, TTX (1 μM; Tocris) to block voltage gated Na^+ channel, NMDA (50 μM; Tocris), glycine (5 μM) and TTX (1 μM) cocktail to induce the Ca^{2+} influx mediated dispersal of $GABA_AR$, DHPG (5 μM; Tocris) to enhance mGluR activity, dynasore (80 μM; Tocris) to prevent dynamin-dependent endocytosis, CysA (1 μM; Santa Cruz, CA, USA) and FK506 (1 μM; Tocris) to inhibit calcineurin activity, Gö6976 (500 nM; Calbiochem) to inhibit Ca^{2+} dependent PKC, PMA to activate PKC, and 4α-PMA as an inactive analogue of PMA (200 nM; Enzo Life Sciences inc. NY, USA). Stock solutions of 2APB, CysA, Gö6976, PMA and 4α-PMA were prepared in DMSO; other drugs were prepared in water. Neurons were acutely exposed to the different drugs for the indicated duration at 37°C in imaging medium comprising MEM without phenol red (Life Technologies), 20 mM HEPES, 33 mM glucose, 2 mM glutamine, 1 mM sodium pyruvate, and B27. To remove Ca^{2+} in the imaging medium (Fig. S1 C-D), MEM were pre-incubated with chelating resin Chelex (Bio Rad) for 60 min at room temperature before adding other components.

Immunocytochemistry and quantitative analysis

Immunochemical detection of $GABA_AR\gamma2$ subunit and gephyrin in cultured neurons was done as previously described (Bannai et al., 2009; Niwa et al., 2012). Endogenous $GABA_AR\gamma2$ subunits were labeled with a rabbit anti- $GABA_AR\gamma2$ subunits antibody (Niwa et al., 2012) by incubating live cells for 30 min at 37°C with 2.0 μg/ml of antibody diluted in imaging medium. Cells were then fixed for 15 min at room temperature (RT; 24–26°C) in paraformaldehyde (PFA; 4% w/v) solution prepared in PBS-0.02% NaN_3. Cells were permeabilized with triton X-100 (0.1% v/v) for 3 min at RT and the nonspecific staining was blocked with bovine serum albumin (BSA; 5% w/v; Sigma-Aldrich, MO, USA) for 30 min at RT. Neurons were then incubated with the mouse anti-synapsin I antibody (1:3000; Synaptic Systems, Goettingen, Germany) or guinea pig anti-PKCα antibody (1 μg/ml; Frontier institute,

Japan) or guinea pig anti-PKCβII antibody (1 μg/ml; Frontier institute) or guinea pig anti-PKCγ antibody (1 μg/ml; Frontier institute) in 2.5% BSA for 60 min at RT. After washes, the cells were incubated for 30 min at RT in Alexa Fluor®-conjugated secondary antibodies (5–10 μg/ml, Alexa Fluor 488 or Alexa Fluor 594; Life Technologies), washed, and mounted on slides with Vectashield (Vector Laboratories, CA, USA). For gephyrin labeling, cells were fixed immediately after the drug treatment and followed by permealization and blocking. Cells were incubated for 90 min at RT with the mouse anti-gephyrin antibody (0.33 μg/ml, clone mAb7a; Synaptic Systems) and the rabbit polyclonal anti-synapsin I antibody (1:400; Merck Millipore, MA, USA). The primary antibodies were visualized with secondary Alexa Fluor 488 goat anti-mouse and Alexa Fluor 594 goat anti-rabbit antibodies (5–10 μg/ml; Life Technologies).

Immunofluorescent images from isolated neurons were acquired on an inverted microscope (IX-70; Olympus, Tokyo, Japan) equipped with a Plan Apo 60× oil immersion objective with a numerical aperture (NA) of 1.42 (Olympus), a cooled CCD camera (Orca-II-ER; Hamamatsu Photonics, Shizuoka, Japan), and appropriate filter sets for Alexa Fluor 488 (ex: 480 ± 10 nm, em: 530 ± 20 nm) and Alexa Fluor 594 (ex: 535 ± 15 nm, em: 580 nm long pass). All images from the same culture were acquired with the same sub-saturation exposure time.

Quantification of synaptic $GABA_AR$-, gephyrin-, synapsin and PKC-associated immunofluorescence was performed using "Integrated Morphometry Analysis" function of the MetaMorph software (Molecular Device Japan, Tokyo, Japan) as previously described (Bannai et al., 2009; Charrier et al., 2006; Levi et al., 2004; Levi et al., 2008; Niwa et al., 2012). $GABA_AR$- and gephyrin-immunoreactive clusters and synapsin-positive presynapses were defined by processing images with multidimensional image analysis (MIA) interface, i.e., a 2D object segmentation by wavelet transform (Racine et al., 2007) and "auto threshold for light object (isodata method)" function of MetaMorph. Synaptic $GABA_AR$ or gephyrin clusters were defined as clusters that overlapped at least 1 pixel with presynaptic terminals. The fluorescence intensity of $GABA_AR$ or gephyrin clusters was defined as the mean fluorescence intensity per cluster multiplied by the mean area per cluster. For PKC immunofluorescence showing diffuse labeling, we measured the fluorescence intensity per pixel of PKC overlapping with $GABA_AR$ clusters. All the data reported here showed same tendency in independent experiments using more than 3 independent culture sets. For population data, data values from 10 or more cells were divided by the average of control levels for that batch, and pooled for statistical analysis.

Time-lapse imaging of mRFP-gephyrin cluster

Time-lapse video microscopy was performed on hippocampal neuron cultures prepared from mRFP-gephyrin expressing knock-in mice (Machado et al., 2011) and as described before (Hanus et al., 2006). Experiments were performed on 19-20 DIV neurons and MEM recording medium (Phenol red-free MEM, 33 mM glucose, 20 mM HEPES, 2 mM glutamine, 1 mM sodium pyruvate, and 1× B27) was used. Time-lapse imaging was carried out on an inverted Nikon Eclipse Ti microscope equipped with a 100× oil-immersion objective (NA 1.49) and excitation / emission filter (FF01-560/25 / FF01-607/36, Semrock) using an Andor iXon EMCCD camera (image pixel size, 160 nm, 300 ms exposure time) in a controlled environment maintained at 35ºC.

Electrophysiology

Whole cell patch clamp experiments on primary cultured neurons were carried out with following solutions. The internal solution contained (in mM): $CsCl_2$, 140; EGTA, 0.2; HEPES, 10; Mg-ATP, 2; GTP-Tris, 1; Na-phosphocreatine, 2.5 (pH 7.2-7.3, 280-290 mOsm). The extracellular recording solution contained (in mM): NaCl, 147; KCl, 2.1; HEPES, 8.8; D-glucose, 8.8; $CaCl_2$, 1.1; $MgCl_2$, 1.1; Pyruvic Acid, 0.026%(v/v) (pH 7.4, 310 mOsm).

Hippocampal brain slices were prepared from postnatal day 14 to 21 BL56/J IP3R1-/- mice and WT littermates. Mice were anesthetized with isoflurane and decapitated, and the brain was rapidly removed and transferred to ice cold cutting solution containing in mM: Choline-Cl, 120; KCl, 3; D-Glucose, 20; $MgCl_2$, 8; NaH_2PO_4, 1.25; $NaHCO_3$, 26; bubbled with 95% O_2/5% CO_2. Acute slices (300 µm thick) were cut on a VT1000S Vibratome (Leica), transferred at 34°C for 15-20min to artificial cerebrospinal fluid (aCSF) containing in mM: NaCl, 125; KCl, 2.5; D-Glucose, 25; $CaCl_2$, 2; $MgCl_2$, 1; NaH_2PO_4, 1.25; $NaHCO_3$, 25; 320 mOsm, bubbled with 95% O_2/5% CO_2, pH 7.35. Slices were allowed to recover, for at least one hour at RT before use. For experiments on acute slice, the internal solution contained (in mM): $CsCl_2$, 130; EGTA, 10; $CaCl_2$, 1; $MgCl_2$, 1; HEPES, 10; Mg-ATP, 2; GTP-Tris, 0.1; Na-phosphocreatine, 2.5 (pH 7.4, 290-300 mOsm). The extracellular recording solution was the aCSF solution.

Spontaneous mIPSCs were recorded in the whole-cell voltage-clamp configuration, in the presence of 2,3-Dihydroxy-6-nitrobenzo[f]quinoxaline-7-sulfonamide (NBQX, 10 µM), D-2-Amino-5-phosphonopentanoic acid (D-AP5, 50 µM), and TTX (1 µM). When required the extracellular recording solution was supplemented with 250 µM MCPG or vehicle (NaOH). Whole-cell patch pipettes (3-5 MΩ) were pulled on a P-97 Micropipette Puller (Sutter Instruments), coated with sylgard-184/R6101 (Dow Corning), and filled with internal solution. All experiments were performed at room temperature.

Whole-cell recordings were obtained using AxopPatch 200B (Axon Instruments) amplifier and acquired with a Digidata1322A A/D converter (Axon Instruments) controlled by pClamp 9 (Axon Instruments). Signals were low-pass filtered at 5/10 kHz and acquired at 50/100 kHz. Series resistance and capacitance were corrected/compensated 70-80%. The membrane potential was held at −70 mV (junction potential left uncorrected). Under these recording conditions GABAergic chloride currents were recorded as inward currents. Detection of individual mIPSC was performed offline using the template-matching event detection algorithm in Clamp fit 9.2 (Axon Instruments). To avoid bias due to a different number of events from each recording, the same number of mIPSC events for each cell was taken from the beginning of the recording, for statistical analysis.

Production of a rabbit $GABA_AR$ β3 subunit antiserum

The rabbit anti-$GABA_AR$ β3 subunit antibody (anti-$GABA_AR$ β3) was raised as described previously (Todd et al., 1996). Purified fusion protein consisting of maltose-binding protein (MBP) and amino acids 345–408 of the mouse $GABA_AR$ β3, part of intracellular loop between transmembrane domains M3 and M4, were injected into rabbits to raise the antibody by the Support Unit for Animal Resources Development at the RIKEN BSI RRC. To obtain fusion proteins, the DNA sequence corresponding to amino acid 345-408 of the $GABA_AR$ β3 was amplified by PCR using FANTOM3 clone C630014N19 from RIKEN Genomic Sciences Research Complex as a template (Carninci et al., 2005), and subcloned into pMAL-C vector (New England Biolabs, MA, USA). Recombinant MBP fusion proteins were expressed in *E. coli* BL21 and purified with amylose resin (New England Biolabs).

The specificity of this antibody was confirmed by Western Blot using cell lysates from HeLa cells (RIKEN BioResource Center, Ibaraki, Japan) transfected with plasmids encoding the α1, β3, and γ2 $GABA_AR$ subunits (Niwa et al., 2012) or from extracts of rat hippocampal primary cultures (Fig. S5C). HeLa cells were cultured in DMEM supplemented with 10% fetal bovine serum and transfected using TransIT-LT1 as described previously (Niwa et al. 2012). Confluent (70–80%) Hela cells cultured on 18 mm coverslips were lysed with 100 µl SDS-PAGE sampling buffer, while rat hippocampal primary cultures were lysed with RIPA buffer as described previously (Bannai et al., 2009) (see "**Surface biotinylation assay**"). The Western blot was done with 1 µg of proteins from 5 µl of cell lysates and using the rabbit $GABA_AR$ β3 serum at 1:2000.

Surface biotinylation assay

Surface biotinylation assay was carried out as previously described (Bannai et al., 2009; Saliba et al., 2007). Neurons were washed twice in PBS (1 mM $CaCl_2$ and 0.5 mM $MgCl_2$), and incubated for 30 min in 0.25 mg/ml sulfo-NHS-SS-biotin (Pierce) followed by 20 min washes in 100 mM glycine to quench excess biotin. Then neurons were lysed in radioimmunoprecipitation assay (RIPA) buffer: 50 mM Tris-HCl (pH7.5), 150 mM NaCl, 1% NP-40, 0.5% sodium deoxycholate, 0.1% SDS, 10 mM EDTA, protease inhibitor cocktail (Roche). Detergent-soluble extracts (150 µg) were incubated for 2 h with immobilized NeutrAvidin (Pierce, 60 µl 1:1 slurry) to purify biotinylated proteins. All steps were done at 4°C.

Western blot

Neurons were treated by SDS sample buffer: 62.5 mM TrisHCl, pH 6.8, 10 (w/v) % glycerol, 2% SDS, 5 (v/v) % β-ME, 0.05% BPB. The following primary antibodies were used: rabbit anti-$GABA_AR$ β3 antiserum (1:2000), rabbit anti-PKCα antiserum (1:100,000; Sigma-Aldrich), guinea pig anti-PKCβII antibody (200 ng/ml; Frontier institute) or guinea pig anti-PKCγ antibody (200 ng/ml concentration; Frontier institute). The primary antibodies were revealed using horseradish peroxidase (HRP)-coupled goat anti-rabbit IgG (1:5000; GE Healthcare Japan, Tokyo, Japan) or goat anti-guinea pig IgG (1:5000; Cappel, CA, USA). Chemiluminescence from HRP reacted to Immobilon Western Chemiluminescent HRP Substrate (Merck Millipore) were detected by Imagequant LAS-4000 mini (GE healthcare) and quantified using Image J.

Ca^{2+} imaging

Ca^{2+} imaging was performed as described previously (Niwa et al., 2012). Neurons were incubated with 0.5 µM fluo-4 AM (Life Technologies) for 5 min at 37°C for loading. Fluo-4 signal was acquired at 0.2 Hz with a 200-ms exposure at room temperature (24–26°C), under an inverted microscope (IX-70; Olympus, JP) equipped with a 40× objective (NA 0.85, UPlanApo; Olympus), a cooled CCD camera (Orca-II-ER; Hamamatsu Photonics), and filters (ex, 480 ± 10 nm; em, 530 ± 20 nm). The ratio of the fluorescence intensities F/F0, where F is a fluorescence intensity and F0 is the intensity at t = 0, was obtained after subtraction of the background fluorescence.

QD-SPT experiments

QD labeling and SPT of $GABA_ARs$ and mGluR5s were performed as previously described (Bannai et al., 2006). Neurons were incubated with our rabbit anti-$GABA_AR\gamma2$ antibody (2.0 µg/ml) or anti-mGluR5 antibody (1.9–2.8 µg/ml) for 5 min, washed, and incubated with the biotinylated anti-rabbit Fab antibody (2.2 µg/ml; Jackson ImmunoResearch, PA, USA) for 5 min. Following washes, the coverslips were incubated with 1.0 nM streptavidin-coated QDs emitting at 605 nm or 625 nm (Life Technologies) in borate buffer for 1 min. After washes, functional presynaptic boutons were labeled with 2 µM FM4-64 (Life Technologies) in imaging medium containing 40 mM KCl for 15 s. Incubation with antibodies and washes were performed at 37°C in imaging medium.

Recording of $GABA_AR$-QD behavior and FM4-64 signals was performed at 37°C in the imaging medium using an inverted microscope (IX-70, -71 or -73 Olympus) equipped with an oil immersion objective (60×, NA > 1.42, Olympus) and a cooled-CCD camera (ORCA-II-ER, Hamamatsu Photonics) or an EM-CCD camera (Cascade, Roper Scientific; ImagEM, Hamamatsu Photonics). Fluorescent signals were detected using appropriate filter sets for QD (ex: 455 ± 70 nm, em: 605 ± 20 nm) and FM4-64 (ex: 535 ± 15 nm, em: 580 nm long pass). QD movies were recorded with an integration time of 76 ms with 512 consecutive frames

(38.9 s), or 200 frames for IP_3R1KO neurons. All recordings were finished within 30 min after labeling.

SPT data analysis

QD-SPD data were analyzed using TI workbench software written by Dr. T. Inoue (Waseda University) as described previously (Bannai et al., 2009; Niwa et al., 2012). $GABA_AR$-QD localization was determined by fitting QD images with a Gaussian model of the point spread function, and the trajectories were reconstructed. Only signals from single QDs with blinking were analyzed. The synaptic area was defined by processing FM4-64 images with wavelet decomposition (Racine et al., 2007). "synaptic" $GABA_AR$-QD trajectories were defined when they overlap with synaptic area + 2 pixels (284 nm). The $GABA_AR$-QD dwell time inside the synapse was defined as the duration of synaptic sub-trajectories.

Diffusion parameters, such as the diffusion coefficient and confinement size, were obtained from the mean square displacement (MSD) plot versus time (MSD-nτ *plot)* that were calculated for $GABA_AR$-QD trajectory by applying the following equation:

$$MSD(n\tau) = \frac{1}{N-n}\sum_{i=1}^{N-n}\left[\left(x\left((i+n)\tau\right)-x(i\tau)\right)^2+\left(y\left((i+n)\tau\right)-y(i\tau)\right)^2\right] \text{(Eq. 1)}$$

((Saxton and Jacobson, 1997)), where xi and yi are the positions of $GABA_AR$-QD in frame i, N is the total frame number, τ is the acquisition time in one frame (76 ms), and nτ is duration over which the displacement is calculated. Diffusion coefficients (*D*) were calculated by fitting first four points excluding the origin of the MSD-nτ plot with the following equation:

$MSD(n\tau) = 4Dn\tau + b$ (Eq. 2),

where *b* is a constant representing localization accuracy (Ehrensperger et al., 2007). The confinement domain size was obtained by fitting the MSD-nτ plot to the following equation:

$$MSD(n\tau) = \frac{L^2}{3}\left(1-\exp\left(-\frac{12Dn\tau}{L^2}\right)\right)+4D_{mac}n\tau \text{ (Eq. 3)}$$

(Kusumi et al., 1993), where L^2 is the estimated maximal area of diffusion when diffusion is confined, and D_{mac} is the diffusion coefficient on a long time scale. The diffusion of $GABA_AR$-QD with MSD-nτ plot that does not apply $|D\text{-}D_{mac}| < 0.1 \times D$ or $L < 0.001$ was defined as restricted motion, and only $GABA_AR$-QDs meeting this criteria were considered for calculations of confinement domain sizes (Ehrensperger et al., 2007). The sub-trajectories shorter than 29 frames were excluded for the calculation of D and L.

$GABA_AR$ γ2 mutant analysis

The $GABA_AR$ γ2L subunit was sub-cloned into pCDNA3.1zeo(+) as described previously (Niwa et al., 2012), and a *PstI* site, corresponding to amino acid LQ, were introduced between amino acids 4 and 5 of γ2L as previously described (Kittler et al., 2000). A Myc-epitope sequence (EQKLISEEDL) was then inserted into this *PstI* site to allow specific QD labeling of mutant γ2L through the myc tag. Point mutations on S327/343 (Fig.S7A) were introduced as described previously (Sawano and Miyawaki, 2000). Plasmid DNAs were transfected using Lipofectamine 2000 (Life technologies) at 3-4 DIV and QD-SPT was carried out 2 days after transfection. To label $GABA_AR$γ2 mutants, anti-Myc tag antibody, clone 4a6 (1:500, Merck Millipore) and biotinylated anti-mouse Fab antibody (2.6 μg/ml; Jackson ImmunoResearch, PA, USA) were used.

Statistical analysis and image preparation

Statistical analyses were performed using the Mann–Whitney *U* test, Welch's *t*-test, and Tukey's range test in ANOVA, with KaleidaGraph (Synergy Software, PA, USA). The numbers of QDs analyzed are shown in Table S1. Images were prepared for printing using

MetaMorph, TI Workbench, Microsoft Excel, Adobe Photoshop, and Adobe Illustrator.

2. Reference for Supplemental Experimental Procedures

Bannai, H., Levi, S., Schweizer, C., Dahan, M., and Triller, A. (2006). Imaging the lateral diffusion of membrane molecules with quantum dots. Nat Protoc *1*, 2628-2634.

Bannai, H., Levi, S., Schweizer, C., Inoue, T., Launey, T., Racine, V., Sibarita, J.B., Mikoshiba, K., and Triller, A. (2009). Activity-dependent tuning of inhibitory neurotransmission based on GABAAR diffusion dynamics. Neuron *62*, 670-682.

Calamai, M., Specht, C.G., Heller, J., Alcor, D., Machado, P., Vannier, C., and Triller, A. (2009). Gephyrin oligomerization controls GlyR mobility and synaptic clustering. J Neurosci *29*, 7639-7648.

Carninci, P., Kasukawa, T., Katayama, S., Gough, J., Frith, M.C., Maeda, N., Oyama, R., Ravasi, T., Lenhard, B., Wells, C.*, et al.* (2005). The transcriptional landscape of the mammalian genome. Science *309*, 1559-1563.

Charrier, C., Ehrensperger, M.V., Dahan, M., Levi, S., and Triller, A. (2006). Cytoskeleton regulation of glycine receptor number at synapses and diffusion in the plasma membrane. J Neurosci *26*, 8502-8511.

Ehrensperger, M.V., Hanus, C., Vannier, C., Triller, A., and Dahan, M. (2007). Multiple association states between glycine receptors and gephyrin identified by SPT analysis. Biophys J *92*, 3706-3718.

Goslin, K., Asmussen, H., and Banker, G. (1998). Rat hippocampal neurons in low-density culture. In Culturing nerve cells, G. Banker, and K. Goslin, eds. (Cambridge: MIT press), pp. 339-370.

Kittler, J.T., Wang, J., Connolly, C.N., Vicini, S., Smart, T.G., and Moss, S.J. (2000). Analysis of GABAA receptor assembly in mammalian cell lines and hippocampal neurons using gamma 2 subunit green fluorescent protein chimeras. Mol Cell Neurosci *16*, 440-452.

Kusumi, A., Sako, Y., and Yamamoto, M. (1993). Confined lateral diffusion of membrane receptors as studied by single particle tracking (nanovid microscopy). Effects of calcium-induced differentiation in cultured epithelial cells. Biophys J *65*, 2021-2040.

Levi, S., Logan, S.M., Tovar, K.R., and Craig, A.M. (2004). Gephyrin is critical for glycine receptor clustering but not for the formation of functional GABAergic synapses in hippocampal neurons. J Neurosci *24*, 207-217.

Levi, S., Schweizer, C., Bannai, H., Pascual, O., Charrier, C., and Triller, A. (2008). Homeostatic regulation of synaptic GlyR numbers driven by lateral diffusion. Neuron *59*, 261-273.

Matsumoto, M., Nakagawa, T., Inoue, T., Nagata, E., Tanaka, K., Takano, H., Minowa, O., Kuno, J., Sakakibara, S., Yamada, M.*, et al.* (1996). Ataxia and epileptic seizures in mice lacking type 1 inositol 1,4,5-trisphosphate receptor. Nature *379*, 168-171.

Niwa, F., Bannai, H., Arizono, M., Fukatsu, K., Triller, A., and Mikoshiba, K. (2012). Gephyrin-independent GABA(A)R mobility and clustering during plasticity. PLoS One *7*, e36148.

Racine, V., Sachse, M., Salamero, J., Fraisier, V., Trubuil, A., and Sibarita, J.B. (2007). Visualization and quantification of vesicle trafficking on a three-dimensional cytoskeleton network in living cells. J Microsc *225*, 214-228.

Saliba, R.S., Michels, G., Jacob, T.C., Pangalos, M.N., and Moss, S.J. (2007). Activity-dependent ubiquitination of GABA(A) receptors regulates their accumulation at synaptic sites. J Neurosci *27*, 13341-13351.

Sawano, A., and Miyawaki, A. (2000). Directed evolution of green fluorescent protein by a new versatile PCR strategy for site-directed and semi-random mutagenesis. Nucleic Acids Res *28*, E78.

Saxton, M.J., and Jacobson, K. (1997). Single-particle tracking: applications to membrane dynamics. Annu Rev Biophys Biomol Struct *26*, 373-399.
Todd, A.J., Watt, C., Spike, R.C., and Sieghart, W. (1996). Colocalization of GABA, glycine, and their receptors at synapses in the rat spinal cord. J Neurosci *16*, 974-982.

4. Supplemental Figures and Legends

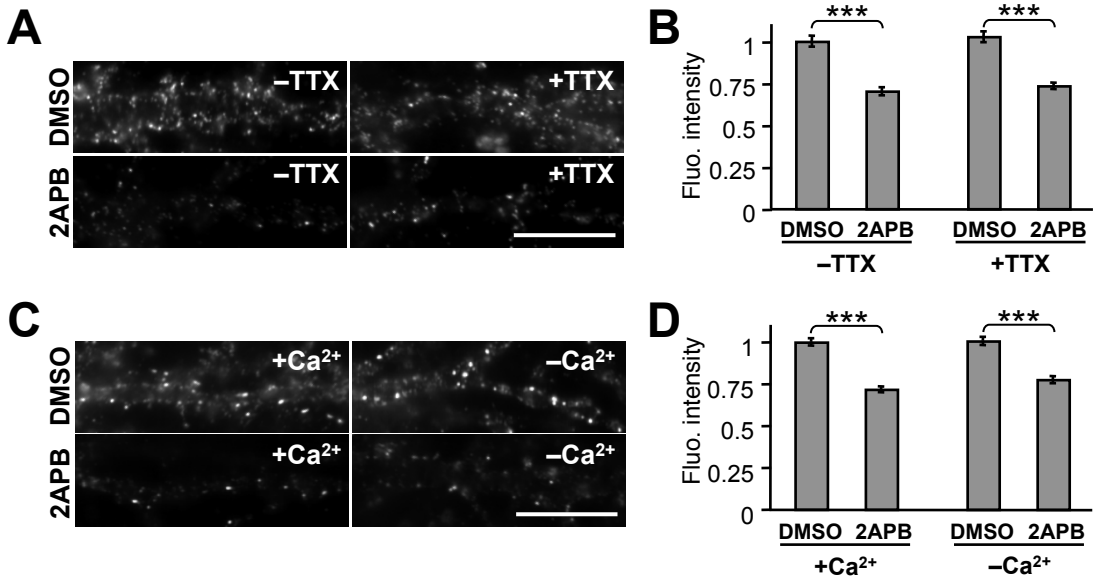

Figure S1. 2APB-induced synaptic $GABA_AR$ decrease is independent of synaptic activity and Ca^{2+} influx

A: Staining for $GABA_AR\gamma2$ of neurons treated with DMSO or 2APB for in the absence or the presence of TTX. **B**: Fluorescent intensities normalized to DMSO without TTX condition (average ± SEM) of synaptic $GABA_AR\gamma2$. **C**: $GABA_AR\gamma2$ cluster after 60 min DMSO or 2APB treatment with or without external Ca^{2+}. **D**: Normalized fluorescence (average ± SEM) of synaptic $GABA_AR\gamma2$. Average fluorescence DMSO with Ca^{2+} condition was assigned as 1. Scale bars: 10 μm. ***: $p < 0.005$, Welch's *t*-test, n = 29–30 cells/condition.

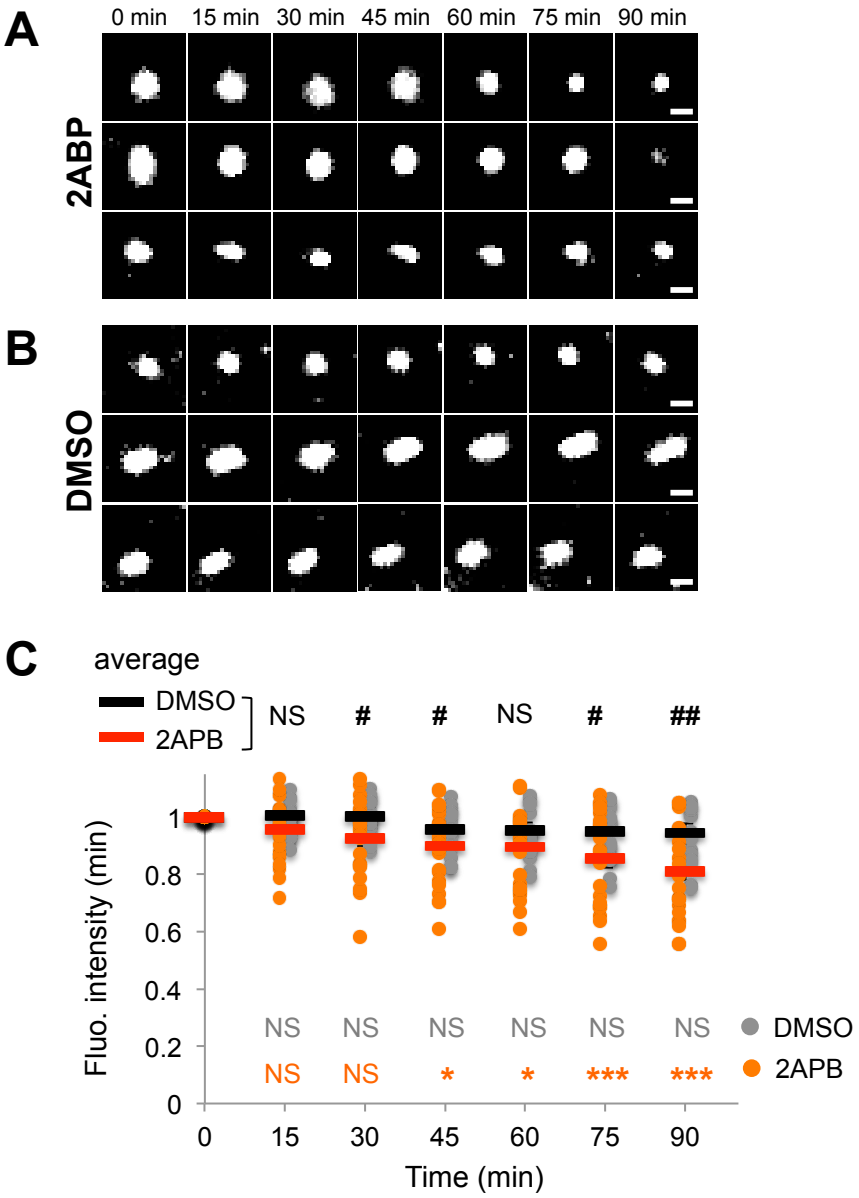

Figure S2. Time-lapse imaging of mRFP-gephyrin clusters

Cultured hippocampal neurons (19-20 DIV) from mRFP-gephyrin knock-in mice treated with 2ABP (100 µM, **A**) or DMSO (**B**). Three representative mRFP-gephyrin clusters shown for 2ABP (**A**) or DMSO (**B**). Scale: 1µm.

C: Time-dependent reduction in cluster fluorescence intensity following 2ABP (orange) but not DMSO (grey) treatment. Bars indicate average value (black: DMSO, red: 2APB).

Bottom: one-way ANOVA with Dunnett's post-hoc test to compare difference from 0 min (grey for DMSO, red for 2APB *: $p<0.05$ / ***: $p<0.001$, NS: non-significant. n= number of movies, DMSO: 15; 2ABP: 24). Top: Unpaired t-test with Welch's correction between DMSO and 2ABP for different time-points (#: $p<0.05$, ##: $p<0.01$, NS: non-significant).

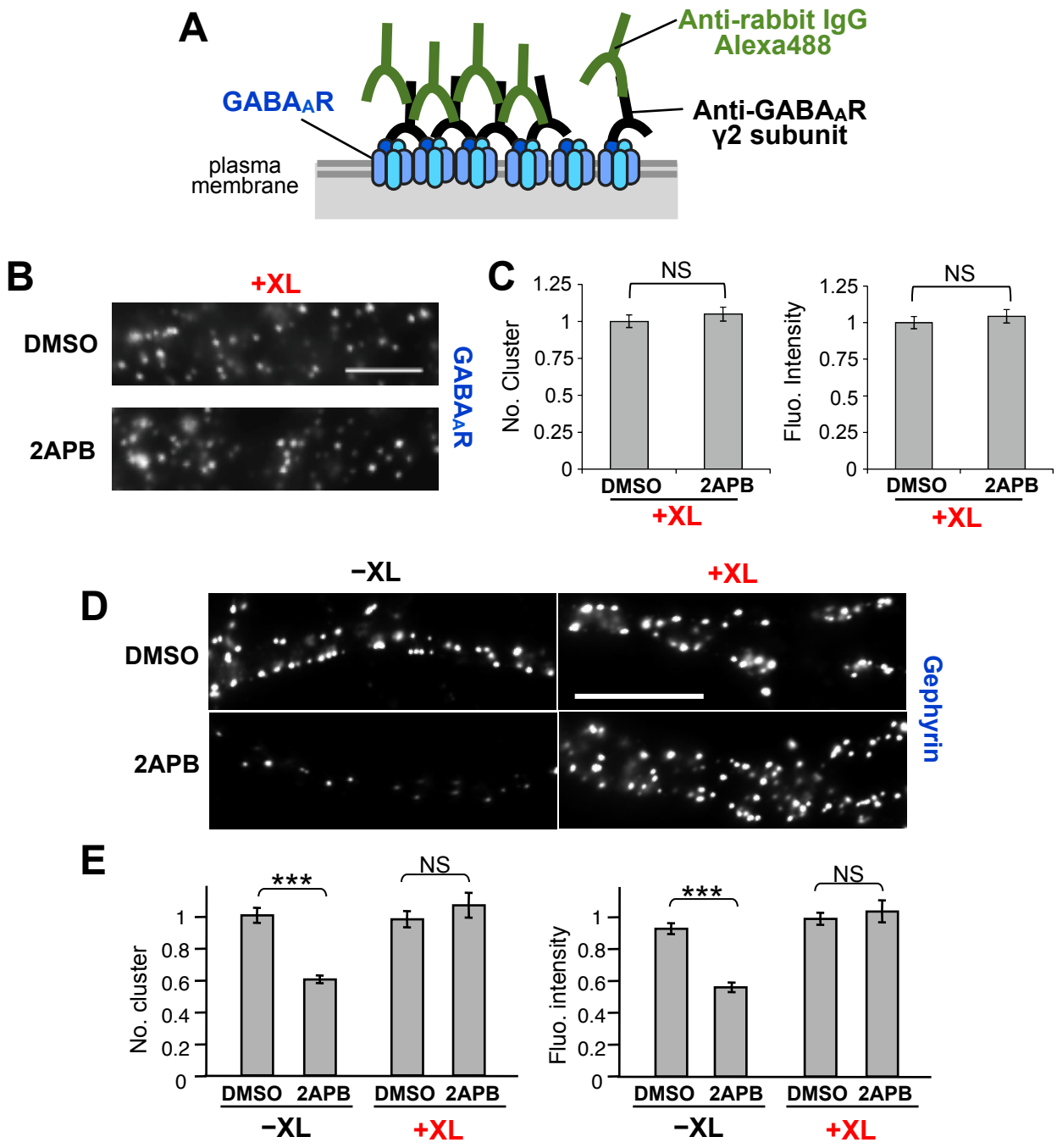

Figure S3. Suppression of 2APB-induced reduction in gephyrin immunofluorescence by $GABA_AR$ immobilization by $GABA_AR$ crosslinking (XL)

A: Diagram of crosslikning (XL). **B**: Examples of $GABA_AR$-immunoreactive clusters in dendrites with or without surface $GABA_AR$ cross-linking (+XL) treated with DMSO or 2APB for 90 min. Scale bar, 5 µm. **C**: Effects of $GABA_AR$ XL and 2APB treatment on the normalized number of clusters (left) and normalized fluorescence intensities (right) of gephyrin clusters (averages ± SEM) n = 30 cells/condition (3 cultures). XL of surface $GABA_AR$ completely inhibited 2APB-induced $GABA_AR$ declustering. **B**: Examples of gephyrin-immunoreactive clusters in dendrites with (+XL) or without (−XL) surface $GABA_AR$ cross-linking treated with DMSO or 2APB for 90 min. Note that 2APB-induced declustering of gephyrin was inhibited by surface $GABA_AR$ XL. Scale bar, 5 µm. **C**: Effects of $GABA_AR$ XL and 2APB treatment on the normalized number of clusters (left) and normalized fluorescence intensities (right) of gephyrin clusters (averages ± SEM). n = 30 cells/ condition (3 cultures). NS: $p > 0.05$; ***: $p < 0.005$, Welch's *t*-test, 2APB-induced reduction in gephyrin cluster size was completely suppressed by $GABA_AR$ XL.

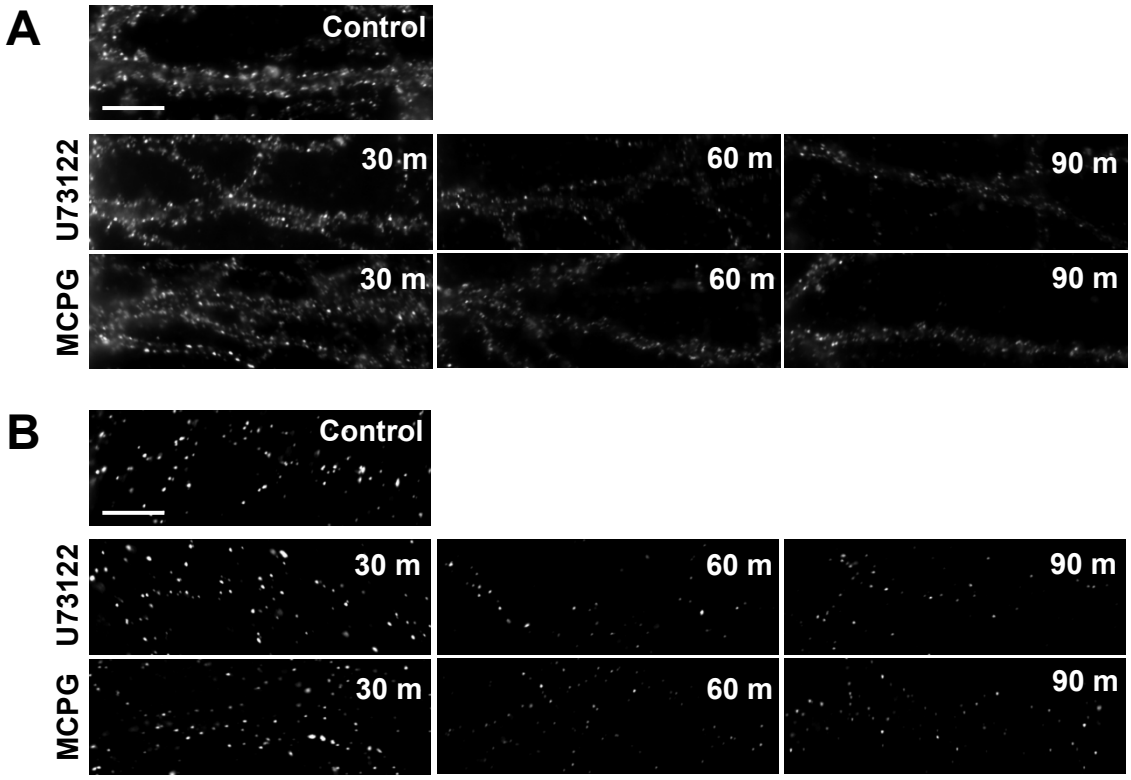

Figure S4. Prolonged blockade of IICR pathway results in declustering of $GABA_AR$ and gephyrin clusters.

Representative examples of immunoreactivity associated with $GABA_AR$ (**A**) and gephyrin (**B**) in the dendrite or rat hippocampal neurons (DIV21–27) of control and those treated 1 μM U73122 and 250 μM MCPG for 30, 60 and 90 min. Scale bar, 10 μm. For quantitative date, see Fig. 2B and D.

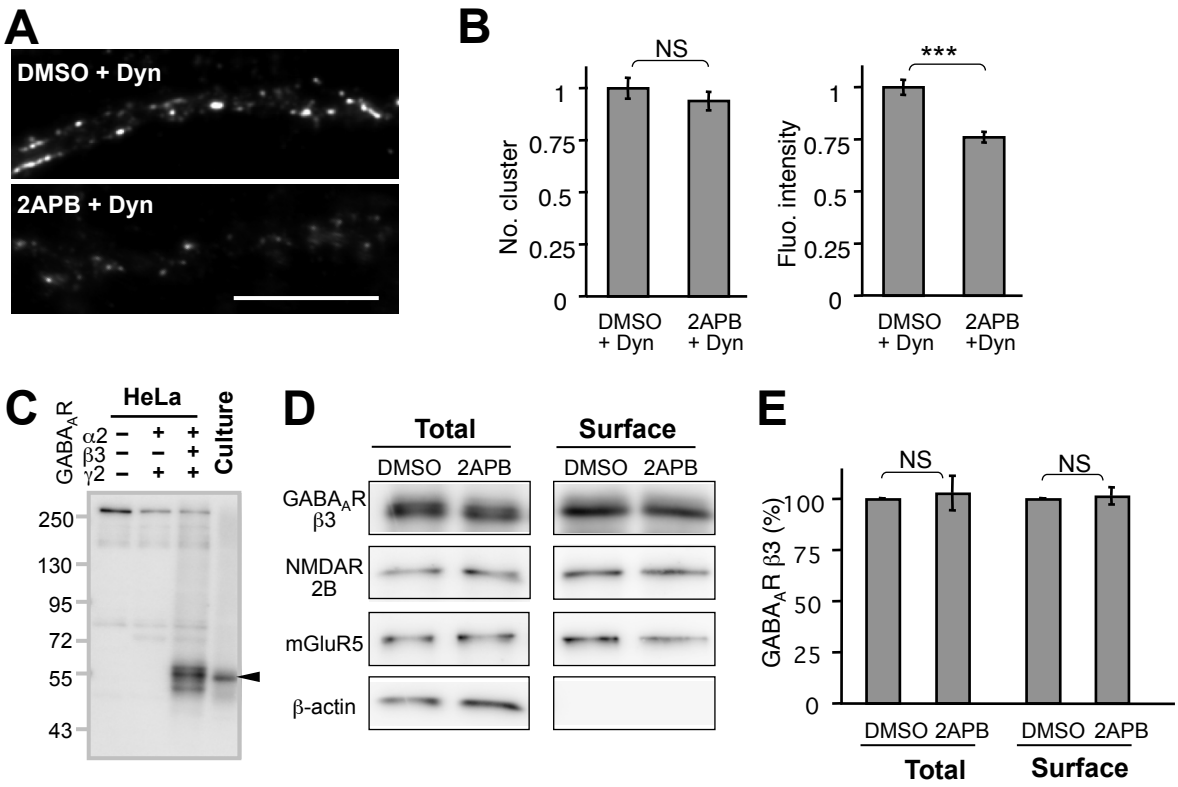

Figure S5. 2APB-induced synaptic $GABA_AR$ reduction is independent of receptor internalization.

A-B: 2APB-induced reduction in synaptic $GABA_AR$ cluster size was observed even in the absence of dynamin-dependent receptor endocytosis. Staining for $GABA_AR\gamma2$ of neurons treated with DMSO or 2APB for in the presence of 80 μM dynasore, a membrane-permeant dynamin inhibitor. **A**: Examples of $GABA_AR$ cluster. Scale bars: 10 μm. **B**: Normalized number of clusters and fluorescent intensity (average ± SEM) of synaptic $GABA_AR\gamma2$. NS: $p > 0.05$, ***: $p < 0.005$, Welch's t-test, n = 30−35 cells/condition. **C**: Westernblot analysis with HeLa cells and rat hippocampal culture lysate using our custom-made anti-$GABA_AR$ β3 antiserum. 55 kDa band (arrowhead) was detected in HeLa cells transfected with plasmids encoding $GABA_AR$ α2, β3, and γ2 subunits and hippocampal culture lysate, but not in non-transfected HeLa cells and those expressing only α2 and γ2 subunits. **D**: Amount of surface expressed biotinylated $GABA_AR$ β3 subunit, NMDAR2B subunit, and mGluR5 are not modified by 60 min 2APB treatment. Biotinylated membrane proteins (surface) isolated from detergent soluble fraction (total) with immobilized Neutroavidin, immunoblotted with antibodies against $GABA_AR\beta3$, NMDAR2B, and actin. **E:** Quantification of total and surface expressed $GABA_AR\beta3$ on DMSO and 2APB- treated cells. Protein level of DMSO condition was assigned as 100%. Both total and surface amount of β3 subunit was equivalent to that in control cells. NS: $p > 0.05$ Welch's *t*-test, n=9.

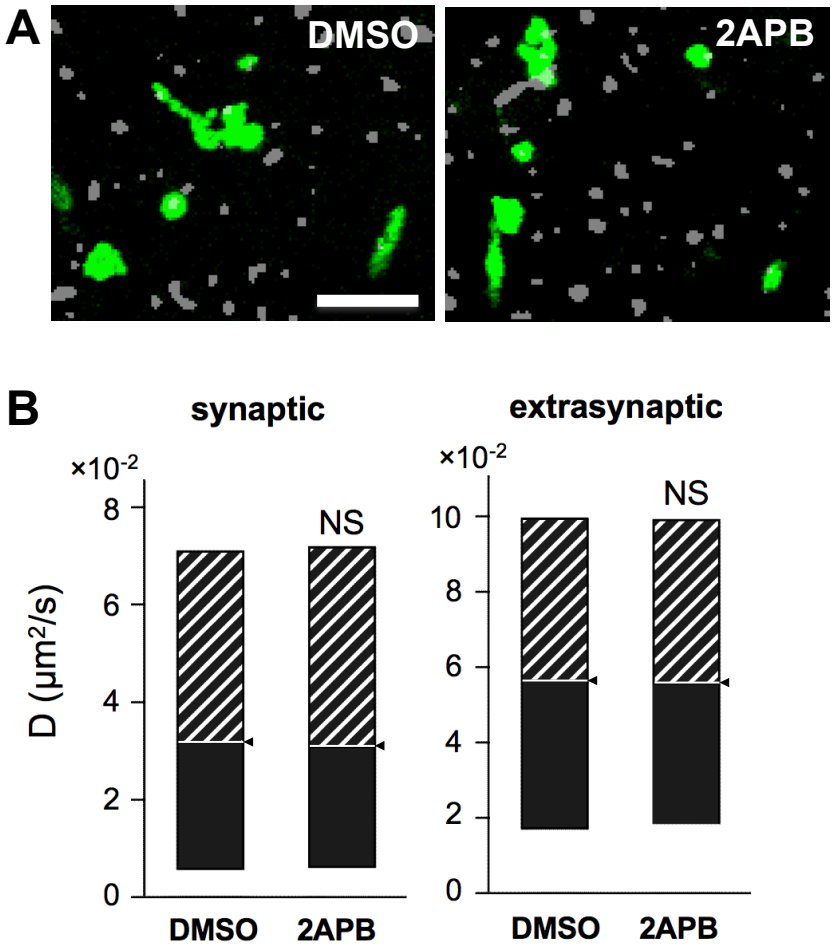

Figure S6. Minor effect of long-term 2APB treatment on lateral diffusion of neuronal mGluR5.

A: Examples of mGluR5-QD trajectories (green), reconstructed from recording sequences of 38.4 s overlaid with FM4-64 signals (gray) in order to identify synapses. Scale bar: 5 µm.
B: Diffusion coefficients (median ± IQR) of mGluR5-QDs inside (left) and outside (right) the synapse after 60-90 min 2APB treatment. NS: $p > 0.05$, Mann-Whitney *U* test. 2APB treatment did not significantly affect the diffusion coefficient of mGlu5s.

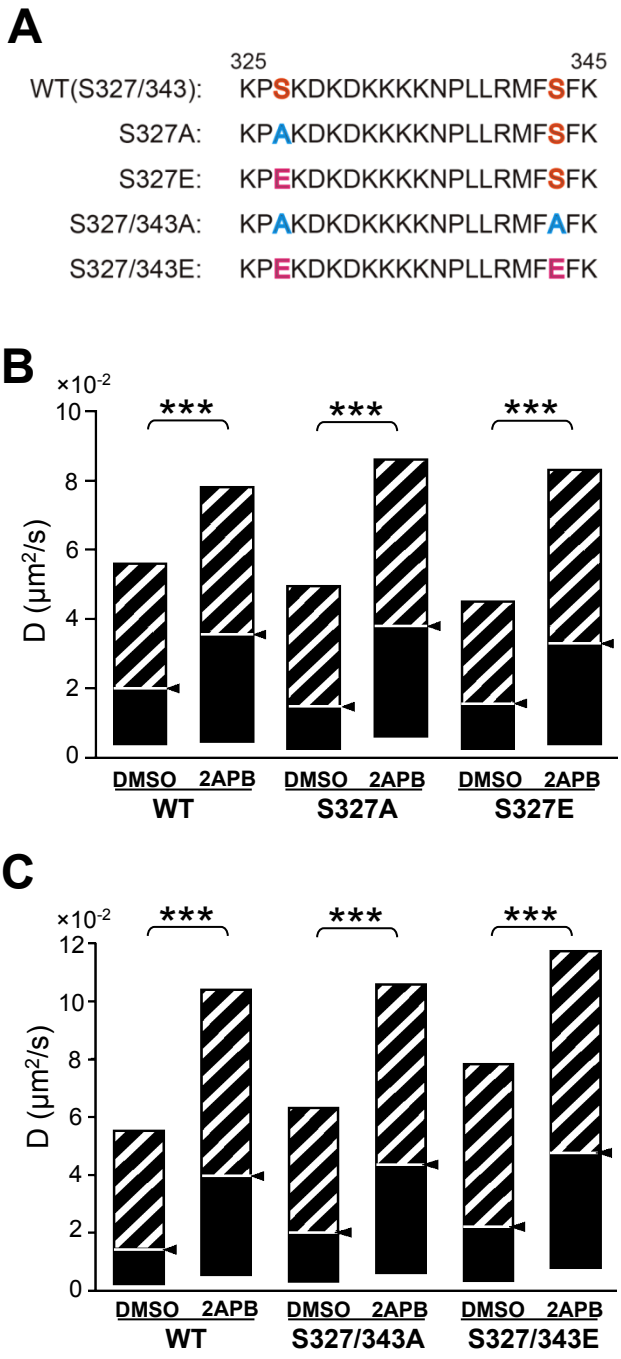

Figure S7. Phosphorylation of S327/343 in $GABA_AR$ γ2 subunit is insufficient to prevent the increase of $GABA_AR$ lateral diffusion caused by inhibition of IICR.

A: Amino acid sequences of a part of cytoplasmic loop region of $GABA_AR$ γ2 subunit. Serine residues shown in brown are S327 and S343 which were mutated into alanine (A, blue) or glutamate (E, magenta). **B**: Impact of 1 h 2APB treatment on diffusion coefficients (median±IQR) of $GABA_ARs$ with or without phospho-mimic mutation in S327. **C**: Diffusion coefficients (median±IQR) of $GABA_AR$ with WT, S327/343A, and S327/343E after 1 h treatment with DMSO or 2APB.
***: $p < 0.005$, Mann-Whitney *U* test. Cells were analyzed at 5-6 DIV.

5. Supplemental Table

Table S1. Number of analyzed $GABA_AR$-QD-trajectories.

Fig. No	Treatment	D (Synaptic)	D (Extra-synaptic)	Dwell time	Conf. size
Fig. 5A–D	**DMSO 0-30 min**	352	793	1337	189
	2APB 0-30 min	404	797	1623	219
Fig. 5E–H	**DMSO 60-90 min**	1031	1540	4091	593
	2APB 60-90 min	867	1253	3761	455
Fig. 5I–L	**WT**	268	550	839	137
	IP_3R1KO	260	637	679	122
Fig. 5M–P	**Control 60-90 min**	487	650	1640	294
	MCPG 60-90 min	672	900	2425	323
Fig. 5Q–T	**DMSO+CysA**	748	n. d.	3109	443
	2APB+CysA	791		2978	470
	DMSO+FK506	377		1383	209
	2APB+FK506	428		1494	248
Fig. 7B–E	**DMSO**	480	n. d.	2097	269
	Gö6976	688		3739	334
Fig. 7F–I	**4α-PMA+DMSO**	601	n. d.	2155	322
	4α-PMA+2APB	458		1947	219
	PMA+DMSO	546		1889	303
	PMA+2APB	546		1831	328
Fig.S6	**DMSO**	370	795	n. d.	n. d.
	2APB	421	853		

Fig. No	Treatment	D (Synaptic + Extra-synaptic)
Fig. S7B	**WT-DMSO**	896
	WT-2APB	646
	S327A-DMSO	751
	S327A-2APB	666
	S327E-DMSO	750
	S327E-2APB	739
Fig. S7C	**WT-DMSO**	1046
	WT-2APB	1167
	S327/343A-DMSO	1083
	S327/343A-2APB	1274
	S327/343E-DMSO	853
	S327/343E-2APB	1651